European Journal of Immunology Clinical·Basic·Translational

Immunodeficiencies and autoimmunity

Basic

Research Article

Junctional adhesion molecule-A deficient mice are protected from severe experimental autoimmune encephalomyelitis

Kristina Berve*, *Julia Michel*, *Silvia Tietz*, *Claudia Blatti*, *Daniela Ivan*, *Gaby Enzmann*, *Ruth Lyck*, *Urban Deutsch*, *Giuseppe Locatelli* and *Britta Engelhardt

Theodor Kocher Institute, University of Bern, Bern, Switzerland

In multiple sclerosis and its animal model, experimental autoimmune encephalomyelitis (EAE), early pathological features include immune cell infiltration into the central nervous system (CNS) and blood–brain barrier (BBB) disruption. We investigated the role of junctional adhesion molecule-A (JAM-A), a tight junction protein, in active EAE (aEAE) pathogenesis. Our study confirms JAM-A expression at the blood–brain barrier and its luminal redistribution during aEAE. JAM-A deficient (JAM-A$^{-/-}$) C57BL/6J mice exhibited milder aEAE, unrelated to myelin oligodendrocyte glycoprotein-specific CD4^{+} T-cell priming. While JAM-A absence influenced macrophage behavior on primary mouse brain microvascular endothelial cells (pMBMECs) under flow in vitro, it did not impact T-cell extravasation across primary mouse brain microvascular endothelial cells. At aEAE onset, we observed reduced lymphocyte and CCR2^{+} macrophage infiltration into the spinal cord of JAM-A$^{-/-}$ mice compared to control littermates. This correlated with increased CD3^{+} T-cell accumulation in spinal cord perivascular spaces and brain leptomeninges, suggesting JAM-A absence leads to T-cell trapping in central nervous system border compartments. In summary, JAM-A plays a role in immune cell infiltration and clinical disease progression in aEAE.

Keywords: Blood–brain barrier · Experimental autoimmune encephalomyelitis · Junctional adhesion molecule A · Macrophages · T cells

Additional supporting information may be found online in the Supporting Information section at the end of the article.

Introduction

A tightly regulated homeostatic environment is a prerequisite for proper functioning of central nervous system (CNS) neurons. CNS homeostasis is ensured by the endothelial blood–brain barrier (BBB), which separates the neural tissue from the constantly changing milieu in the bloodstream. The BBB is composed of highly specialized microvascular endothelial cells that prohibit free diffusion of molecules across this barrier by low pinocytotic activity and by a unique series of tight junctions [1]. The BBB also ensures CNS immune surveillance without disturbing CNS homeostasis by strictly controlling immune cell entry into CNS

Correspondence: Prof. Dr. Britta Engelhardt
e-mail: britta.engelhardt@unibe.ch

Kristina Berve and Julia Michel contributed equally.

border compartments like the subarachnoid or perivascular spaces (PVS) [2]. Immune cells within these compartments remain separated from the CNS parenchyma by the glia limitans established by astrocyte end-feet and a parenchymal basement membrane ensheathing the entire CNS parenchyma and establishing an additional barrier for immune cells [3].

In multiple sclerosis (MS) and its animal model, experimental autoimmune encephalomyelitis (EAE), a large number of circulating immune cells enter the CNS parenchyma, resulting in inflammation, BBB breakdown, and demyelination, eventually leading to neurological dysfunction and neurodegeneration.

Immune cell infiltration into the CNS is unique as it requires the crossing of two tissue barriers, namely, the endothelial BBB followed by the glia limitans [4]. Immune cell extravasation across the endothelial BBB is a multistep process that is mediated by the sequential interaction of adhesion and signaling molecules present on the immune cell and on the BBB [5]. During low-inflammatory conditions, diapedesis of immune cells across the BBB at the level of the postcapillary venules preferentially occurs through tricellular junctions [6], whereas transcellular diapedesis is significantly increased during inflammatory conditions, when junctional barrier integrity is compromised [7–9]. Thus, the role of junctional molecules in regulating BBB integrity and the cellular pathways of immune cell diapedesis are distinct [6]. Hence, understanding the unique properties and components of the BBB junctions in this context is essential.

Although all endothelial cells across the vertebrate vasculature form adherens junctions consisting of VE-cadherin/catenin complexes and harbor transmembrane proteins such as platelet-endothelial cell adhesion molecule (PECAM)-1 and CD99 located outside of organized junctional complexes, the BBB endothelium is characterized by additional, molecular unique tight junctions: claudin-5, occludin, and the junctional adhesion molecules (JAM)-A, B, and C form a continuous and complex tight junction network between endothelial cell–cell contacts strictly regulating paracellular diffusion of water-soluble molecules across the BBB [10, 11]. Although claudin-5 is essential for maintaining a barrier for paracellular diffusion [12] and occludin in regulating tight junctional stability and function [13], members of the JAM family play a role in cell polarity [14, 15]. The JAMs are type-I transmembrane glycoproteins of the immunoglobulin superfamily composed of two extracellular domains, one transmembrane part and a short cytoplasmic tail with a PDZ-domain binding motif [16, 17]. Among the JAM members JAM-A is a multifaceted molecule with various physiological functions [18] implicated in tight junction formation and regulation of paracellular permeability [17, 19–21]. JAM-A is localized in tight junctions of endothelial and epithelial cells. In addition, JAM-A is expressed by circulating cells, including monocytes, lymphocytes, neutrophils, platelets, and erythrocytes [16, 19, 22, 23]. Interestingly, JAM-A has been described to control leukocyte adhesion and diapedesis across the vascular endothelium in vitro and in vivo [24, 25].

To fulfill these various functions, JAM-A can engage in *cis* and *trans* homophilic as well as heterophilic interactions, in the case of the latter with the leukocyte integrin LFA-1 or intracellular PDZ-domain containing proteins like ZO-1, AF-6, or PAR-3 [26, 27]. Local redistribution from the tight junctions to the apical surface of endothelial cells upon various inflammatory conditions allows JAM-A to interact with circulating immune cells guiding their diapedesis across the endothelial wall [24, 28, 29].

JAM-A regulates epithelial barrier function as shown by enhanced intestinal epithelial permeability in JAM-A deficient mice [30] or enhanced colonic epithelial permeability after treatment with function-blocking JAM-A antibodies [31]. At the same time, the presence of JAM-A at the tight junctions is suggested to regulate barrier properties of endothelial cells, as shown for the corneal endothelium [20, 32], whereas decreased junctional expression of JAM-A was observed during BBB breakdown in rats with cortical cold injury [33]. Importantly, in MS patients, the loss of vascular JAM-A immunostaining in active and inactive lesions [34] was associated with BBB leakage [35, 36] proposing a central role of JAM-A in BBB integrity. In light of its dual function as a regulator of tight junction integrity and as a cell adhesion molecule regulating immune cell diapedesis [37], JAM-A is an interesting candidate to study in the context of MS pathogenesis. Hence, we here investigated the role of JAM-A in BBB integrity and immune cell diapedesis across the BBB during active EAE (aEAE).

Results

JAM-A immunostaining is enhanced in the CNS vasculature during EAE

To verify expression of JAM-A at the BBB, we performed immunostainings on brain and spinal cord cryosections obtained from C57BL/6J mice suffering from aEAE and healthy control littermates. In the brain of healthy C57BL/6J mice, we detected JAM-A staining in parenchymal microvessels (Fig. 1A), in the choroid plexus (ChP) epithelium and possibly ChP endothelium (Fig. S1A), and in the meningeal vasculature (not shown). In the brain of mice during peak and chronic aEAE (days 18–30 postimmunization; p.i.), the expression pattern was similar, with more JAM-A positive parenchymal vessels detected in non-cortical regions like the striatum (Fig. 1B) and an intensified JAM-A immunostaining on the basolateral side of the ChP epithelium (Fig. S1B). We next performed double immunofluorescence stainings for JAM-A and CD45 on brain cryosections of C57BL/6J mice with aEAE (day 18 p.i.) (Fig. 1C–E). JAM-A was detected on $CD45^{dim}$ microglia cells (Fig. 1C and magnified insets in Fig. 1D) as well as on most (Fig. 1C,D, arrows) but not all (Fig. 1C,D, arrowheads) $CD45^{high}$ infiltrating immune cells. The latter observation was expected because myeloid cells account for the majority of infiltrating immune cells in myelin oligodendrocyte glycoprotein $(MOG)_{aa35–55}$-induced aEAE and have previously been

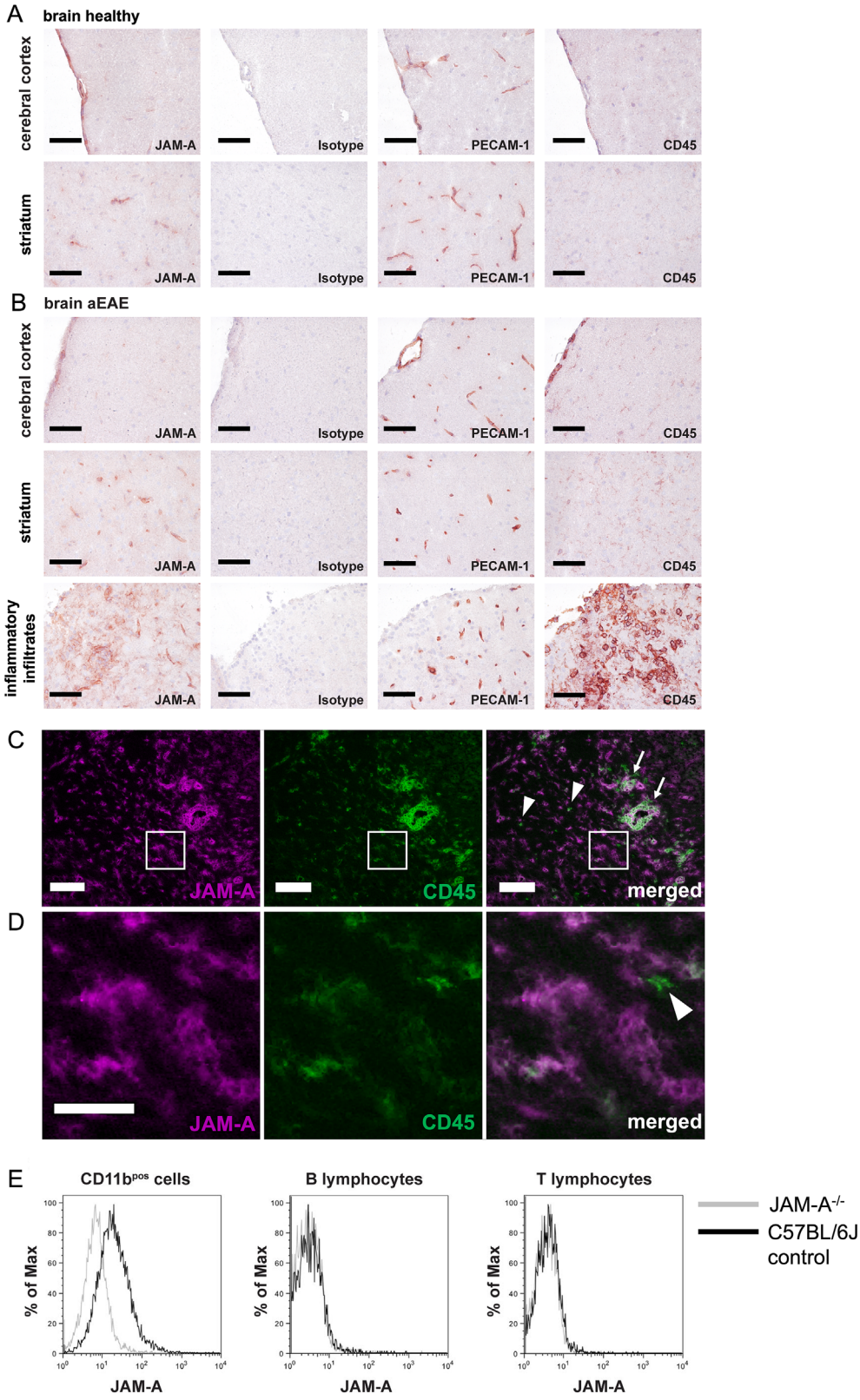

Figure 1. Detection of junctional adhesion molecule-A (JAM-A) in the inflamed blood–brain barrier (BBB) vasculature and on immune cells in the central nervous system (CNS) during active experimental autoimmune encephalomyelitis (aEAE). (A and B) Brain cryosections of (A) healthy C57BL/6J mice and (B) C57BL/6J mice with aEAE were stained with rat antibodies against JAM-A (BV12), isotype control, platelet-endothelial cell adhesion molecule 1 (PECAM-1), or CD45. Two independent stainings were performed with three mice in each group in total. Tissue from aEAE mice was obtained between days 18–30 postimmunization (p.i.), whereas mice showed clinical scores between 1 and 2. Scale bar = 60 µm. (C)

shown to express JAM-A [22, 38]. The JAM-A^{negative}CD45^{high} immune cells detected are probably lymphocytes, as also suggested by our flow cytometry analysis of blood (Fig. 1E), lymph nodes, and spleen (not shown) cell suspensions obtained from C57BL/6J mice with aEAE at disease onset (days 13–15 p.i.). A similar JAM-A staining pattern was observed in spinal cord sections and by employing a different monoclonal rat anti-mouse JAM-A antibody (BV11) (data not shown).

Luminal accessibility of JAM-A at the BBB during health and EAE

Next, we asked if the tight junction protein JAM-A is accessible on the luminal side of the BBB endothelium in vivo to mediate immune cell-endothelial interactions via *trans* homophilic or *trans* heterophilic binding to its potential integrin ligand LFA-1 on circulating immune cells [27]. Therefore, we intravenously (i.v.) injected the monoclonal rat anti-mouse JAM-A antibody (BV12) into healthy C57BL/6J mice as well as C57BL/6J mice at peak of aEAE (days 18–19 p.i.) and analyzed their in vivo binding to the vascular wall by immunostaining for bound rat IgGs in brain and spinal cord cryosections. As a positive control we injected an anti-PECAM-1 antibody, while injecting a nonbinding rat IgG2a antibody served as a negative control (Fig. 2). Parenchymal microvessels in the CNS of healthy mice displayed only some or no luminal JAM-A and PECAM-1 antibody binding (Fig. 2A,E) while applying the respective primary antibodies on the consecutive cryosections allowing to detect also nonluminal antigens, confirmed vascular staining for both, JAM-A and PECAM-1 (Fig. 2B,F). In contrast, during aEAE, we found strong luminal binding of the i.v.-injected anti-JAM-A antibodies to CNS microvessels surrounded by inflammatory cells (Fig. 2C, arrowheads) and, to a lesser extent, to inflamed vessels lacking perivascular inflammatory cuffs (Fig. 2C, arrow). Applying the primary anti-JAM-A antibodies on consecutive sections produced a similar staining pattern and diffuse staining for JAM-A also on CNS infiltrating immune cells and activated microglia (Fig. 2D, arrowheads). Similarly, PECAM-1 was detected on the luminal side of CNS microvessels at sites of immune cell infiltration (Fig. 2G), although more prominent staining of the consecutive section with the respective primary antibody suggests that the majority of PECAM-1 at the BBB is not luminally accessible (Fig. 2H). Specificity of the respective stainings was confirmed by the lack of positive staining after i.v. injection of a rat IgG isotype control antibody (Fig. 2I,K). The inflamed status of the BBB endothelium was confirmed by vascular P-selectin staining at sites of immune cell infiltration (Fig. 2J,L). Furthermore, in contrast to the ChP of healthy mice (Fig. S1A), we found faint luminal JAM-A immunostaining on the fenestrated ChP endothelium in aEAE mice (Fig. S1D, arrows). The majority of JAM-A protein in the ChP was, however, inaccessible for the i.v.-injected antibodies (Fig. S1C).

In summary, our data show that in healthy C57BL/6J mice tight junctional JAM-A is inaccessible to anti-JAM-A antibodies injected into the circulation. However, during aEAE, JAM-A becomes accessible for immune cell interactions, either by increased de novo synthesis or luminal redistribution, as shown previously [39–41]. Additionally, we detected positive immunostaining for JAM-A on the fenestrated vessels in the ChP during aEAE.

Lack of JAM-A ameliorates EAE

As our immunostainings showed that JAM-A is redistributed to the luminal surface of CNS microvessels and upregulated in fenestrated vessels of the ChP during aEAE, we asked if JAM-A is involved in aEAE pathogenesis. To this end, we induced aEAE in JAM-A$^{-/-}$ C57BL/6J mice and their wild-type (WT) littermates and compared the development of the clinical disease. We observed a significant amelioration in overall clinical disease severity in JAM-A$^{-/-}$ C57BL/6J mice compared to their WT littermates as calculated by area under the curve analysis (Fig. 3A,B). The improvement in clinical disease progression was also reflected by a reduced loss in body weight, a standard measure for assessing EAE disease severity, in the absence of JAM-A (Fig. 3C). Furthermore, JAM-A$^{-/-}$ C57BL/6J mice had a slightly reduced disease incidence in comparison to WT C57BL/6J controls (Fig. 3D), as well as a mild delay in day of EAE disease onset (not shown). Taken together these observations underscore a role for JAM-A in aEAE pathogenesis.

MOG-specific T-cell priming is not impaired in JAM-A$^{-/-}$ C57BL/6J mice

As lack of JAM-A ameliorated clinical sings of aEAE, we next asked if JAM-A might be involved in antigen-specific T-cell priming and activation in peripheral secondary immune organs in response to MOG$_{aa35–55}$-immunization. Antigen-recall assays with splenocytes and lymph node cell suspensions isolated from MOG$_{aa35–55}$-peptide/complete Freund's adjuvant (CFA) immunized JAM-A$^{-/-}$C57BL/6J mice and WT littermates at day

Double-immunofluorescence staining for JAM-A (magenta, pseudo-colored) and CD45 (green) on brain cryosections from a C57BL/6J mouse with aEAE (day 18 p.i., clinical score: 1). Arrows point to JAM-A positive and arrowheads to JAM-A negative immune cells. Scale bar = 100 µm. (D) Higher magnification of the insets outlined in the top panel is shown. The arrowhead points to a JAM-A negative immune cell surrounded by JAM-A/CD45 double-positive cells. Scale bar = 40 µm. (E) Cell surface expression of JAM-A on circulating immune cells obtained from the blood of C57BL/6J mice (black line) at aEAE onset (days 13–15 p.i.) and double-stained for JAM-A (BV12) and different markers, including CD11b (myeloid cells), CD19 (B lymphocytes), and CD90.2 (T lymphocytes). Blood of JAM-A$^{-/-}$ C57BL/6J mice (gray line) served as a negative control for the JAM-A staining. Histograms are representative of $N = 2$ experiments, each with four mice per group whose blood was pooled.

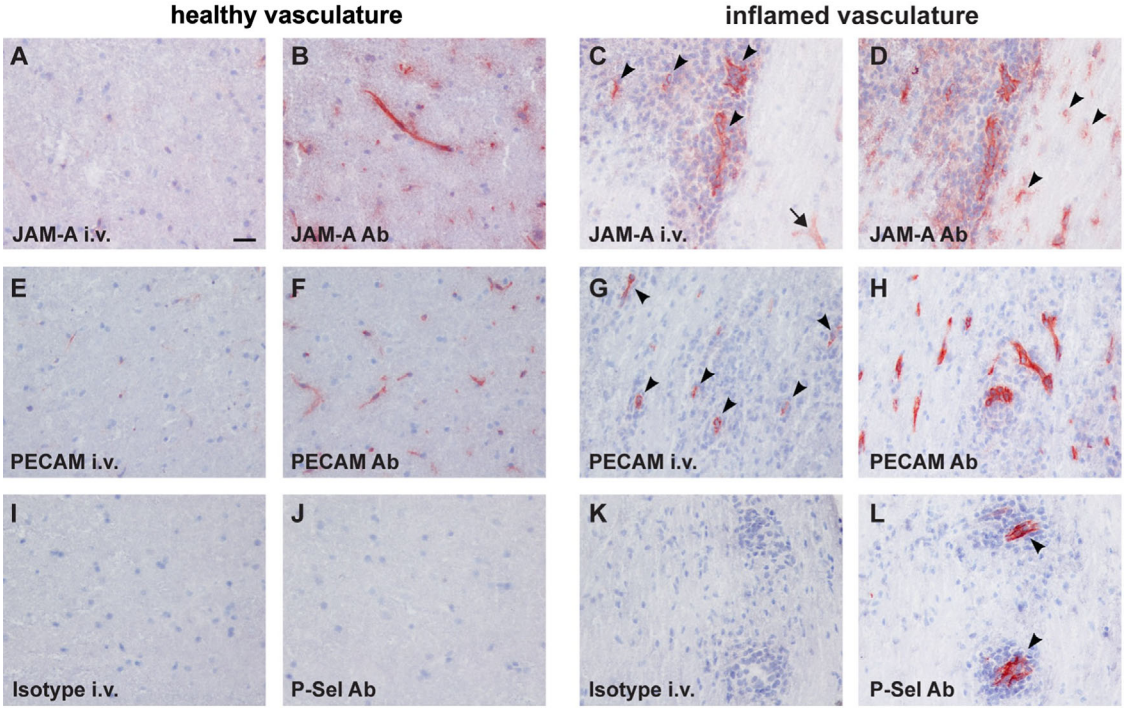

Figure 2. Luminal localization of junctional adhesion molecule-A (JAM-A) on the inflamed blood–brain barrier (BBB) endothelium during active experimental autoimmune encephalomyelitis (aEAE). Healthy C57BL/6J mice and C57BL/6J mice with aEAE were intravenously injected with 60–90 µL containing 100 µg monoclonal rat-anti mouse antibody detecting JAM-A (BV12) (A–D), platelet-endothelial cell adhesion molecule 1 (PECAM-1) (E–H), or an isotype control (I–L). Shown are spinal cord cryosections stained with either anti-rat secondary antibody only (A, C, E, G, I, and K) or primary antibodies against JAM-A (B and D), PECAM-1 (F and H), isotype control (I and K), or P-selectin (J and L) followed by secondary antibody to distinguish between luminal only versus full detection of the respective proteins. Luminal JAM-A immunostaining was found in vessels surrounded by immune cell infiltrates (arrowheads in C) and to a lesser degree in vessels without immune cell infiltrates (arrow in C). The arrowheads in D point at activated microglial cells. For this experiment, each antibody was injected into two healthy and into two mice with aEAE (day 18–19 postimmunization [p.i.], clinical score: 1–2). Scale bar = 25 µm.

14 p.i. revealed comparable proliferation of $CD4^+$ T lymphocytes in response to increasing concentrations of $MOG_{aa35–55}$-peptide (Fig. 4A). The antigen-specific proliferation against the CFA-component PPD as well as the polyclonal activation in response to the mitogen ConA or stimulation with anti-CD3/anti-CD28 antibodies were also indistinguishable in both groups (Fig. 4B). Similar results were obtained when mice were sacrificed before clinical onset of aEAE as early as day 6 or 10 p.i. or when the assay was performed with cell suspensions from blood (data not shown). To exclude that lack of JAM-A affects cell surface expression of other adhesion molecules involved in their migration into the CNS, we performed flow cytometry analysis of T lymphocytes from draining lymph nodes of JAM-$A^{-/-}$ or WT mice with aEAE. We found comparable cell surface expression levels of the integrins CD11a (LFA-1) and CD49d (α_4-integrin), both known to play a role in T-cell migration across the BBB (Fig. S2A). In addition, lack of JAM-A had no influence on the cell surface expression of CD44 and CD62L (L-selectin) (Fig. S2A). Similar results were obtained with T cells isolated from blood and spleen (data not shown). Moreover, the number of $CD4^+$ T cells expressing key cytokines including interferon (IFN)-γ, interleukin (IL)-17A, and granulocyte-macrophage colony-stimulating factor (GM-CSF) isolated from lymph nodes at day 14 p.i. was comparable between WT and JAM-$A^{-/-}$ C57BL/6J mice, whereas IL-4^+ $CD4^+$ T cells were virtually absent (Fig. S2B).

In conclusion, lack of JAM-A did not affect peripheral T-cell priming or antigen-specific T-cell proliferation, adhesion molecule, or cytokine expression levels of $CD4^+$ T cells after induction of aEAE.

Lack of JAM-A does not increase paracellular permeability BBB endothelium in vitro

We next asked if lack of JAM-A affects barrier properties of the BBB. To this end, we compared the paracellular permeability of JAM-$A^{-/-}$ and WT primary mouse brain microvascular endothelial cells (pMBMECs) as an in vitro model for the BBB. Measuring the permeability for the low molecular weight tracers 3 kDa (Fig. 4C) or 10 kDa (Fig. 4D) dextran across unstimulated or tumor necrosis factor (TNF)-α stimulated JAM-$A^{-/-}$ and WT pMBMEC monolayers did not show any significant differences. To exclude a potential compensatory upregulation or redistribution of other members of the JAM family or tight junction molecules in the absence of JAM-A, we performed immunofluorescence stainings for different junctional molecules in JAM-$A^{-/-}$ and WT pMBMECs. Occludin, claudin-5, and ZO-1 showed prominent junc-

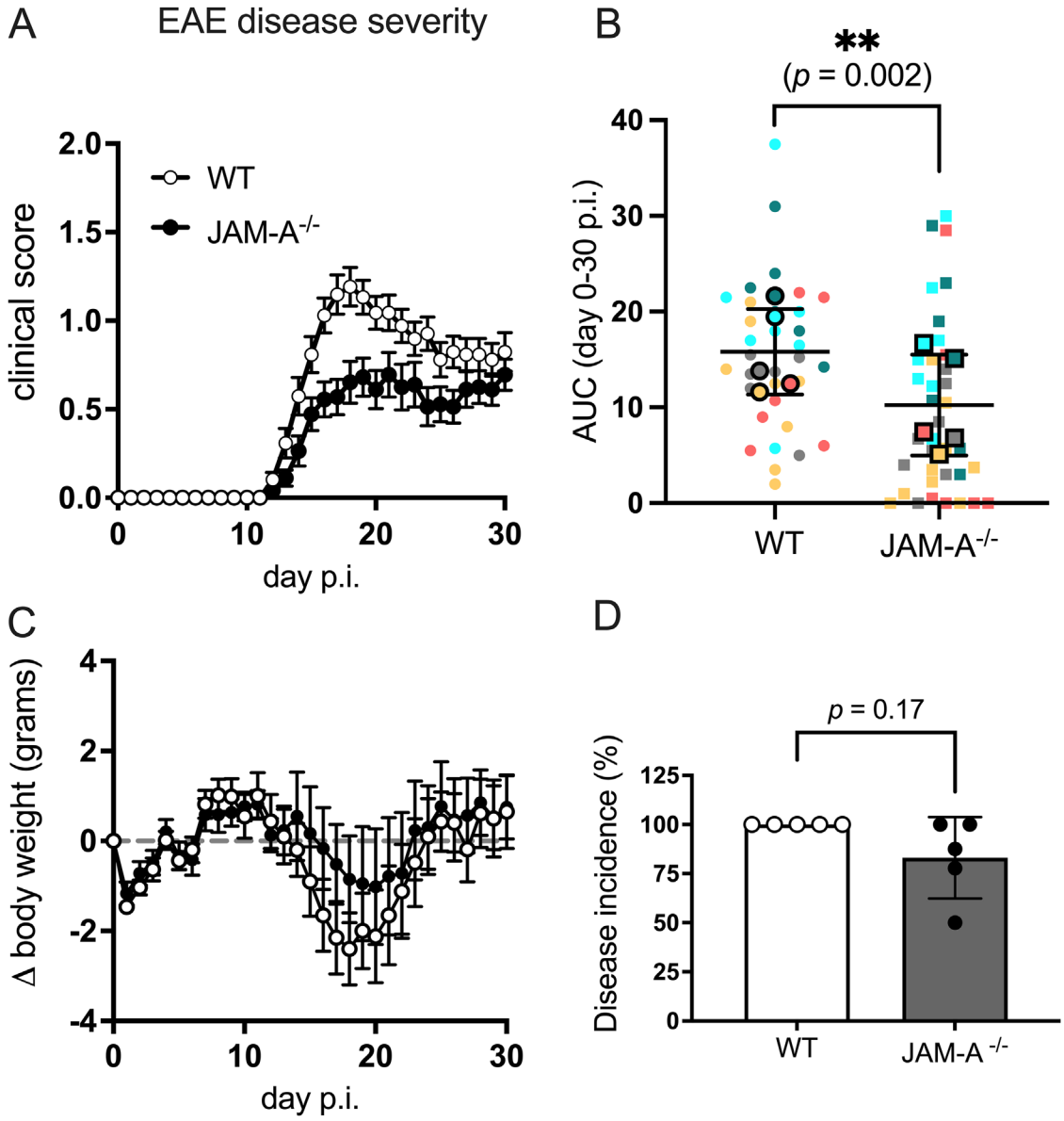

Figure 3. Junctional adhesion molecule-A (JAM-A$^{-/-}$) C57BL/6J mice develop ameliorated active experimental autoimmune encephalomyelitis (aEAE). (A) Average clinical disease course of myelin oligodendrocyte glycoprotein $(MOG)_{aa35-55}$-induced aEAE mice from five independent experiments comparing wild-type (WT) C57BL/6J mice and JAM-A$^{-/-}$ C57BL/6J mice. Mean ± standard error of the mean (SEM) are shown. (B) Overall disease severity as determined by the area under the curve (AUC) in WT C57BL/6J mice and JAM-A$^{-/-}$ C57BL/6J mice from 5 EAE experiments. Depicted are "SuperPlots," which superimpose summary statistics from independent experiments on top of biological replicates: Individual mice were separately pooled for each independent experiment and the mean was calculated for each experiment; means were then used to compare statistical differences across experimental groups. Each mouse is represented as a dot/square that is color-coded according to the respective experiment it is derived from. Mean ± standard deviation (SD) are shown. (C) Changes in body weight compared to the day of aEAE induction (day 0) for all animals per group across 5 independent EAE experiments. Mean ± SEM are shown. (D) Average disease incidence per experiment in percentage from 5 independent EAE experiments. In total 34 WT C57BL/6J mice and 36 JAM-A$^{-/-}$ C57BL/6J mice were used in these experiments. Mean ± SD are shown. (A and C) Each dot represents mean clinical score or mean weight change, respectively, per day and experimental group. (D) Each dot represents one independent EAE experiment. Statistical differences between two groups were calculated using paired (B) or unpaired (D) two-tailed students *t* test. $^{**}p \leq 0.01$.

tional localization, independent of the presence or absence of JAM-A (Fig. S3A). Induction of an inflammatory status of pMBMECs by TNF-α stimulation was confirmed by upregulation of VCAM-1 (Fig. S3B) [42]. In conclusion, JAM-A is dispensable for the maintenance of BBB integrity in vitro.

Lack of JAM-A affects postarrest behavior of macrophages but not T cells on pMBMECs in vitro

JAM-A has been described to mediate adhesion and diapedesis of different leukocyte subsets, including T cells and myeloid cells

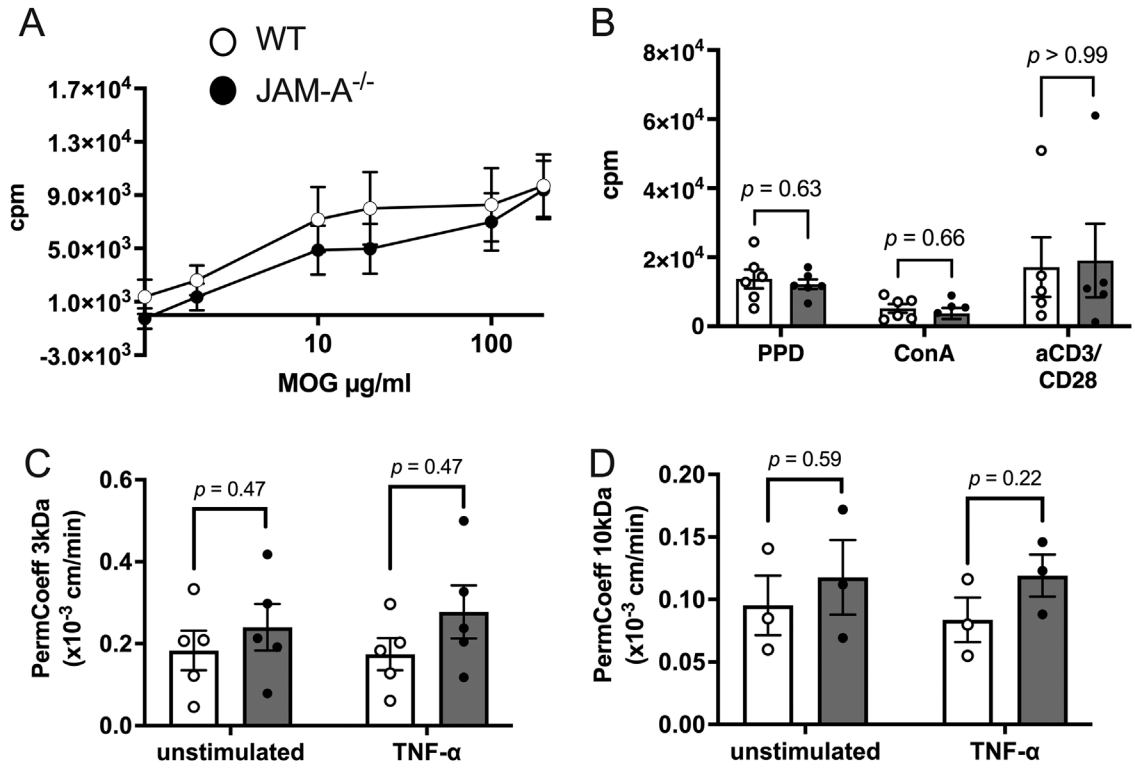

Figure 4. Absence of junctional adhesion molecule-A (JAM-A) does not impair $CD4^+$ T-cell priming or primary brain microvascular endothelial cell permeability in vitro. (A) In vitro proliferation of $CD4^+$ T cells in response to increasing concentrations of myelin oligodendrocyte glycoprotein $(MOG)_{aa35–55}$-peptide (1–200 µg/mL) in primary cultures isolated from draining lymph nodes of wild type (WT) and JAM-$A^{-/-}$ C57BL/6J mice at day 14 postimmunization (p.i.) with $MOG_{aa35–55}$/complete Freund's adjuvant (CFA) and measured by incorporation of $[^3H]$-thymidine is shown. (B) The proliferation of T cells in response to 10 µg/mL of protein purified derivate (PPD) of *Mycobacterium tuberculosis*, the T-cell mitogen ConA or a mixture of anti-CD3 and anti-CD28 (0.1 µg/mL each) is shown for lymph node primary cultures isolated from WT and JAM-$A^{-/-}$ C57BL/6J mice at day 14 p.i. (A and B) T-cell proliferation was normalized to baseline proliferation in medium. $N = 5–6$ experiments. (C and D) Permeability coefficients [$\times 10^{-3}$ cm/min] for (C) 3 kDa ($N = 5$) and (D) 10 kDa ($N = 3$) AlexaFluor680-dextran from unstimulated and tumor necrosis factor (TNF)-α stimulated WT and JAM-$A^{-/-}$ primary mouse brain microvascular endothelial cells (pMBMECs) are shown. Each dot represents one individual experiment except from (A) in which the mean cpm value per $MOG_{aa35–55}$ concentration across 5–6 experiments was calculated. Data are presented as mean ± standard error of the mean (SEM).

across inflamed endothelium in peripheral vascular beds [17, 27, 43, 44]. Performing binding assays of $CD4^+$ T cells on increasing concentrations of immobilized recombinant JAM-A under static conditions showed that T cells can bind with low efficiency to JAM-A when compared to ICAM-1, a well-known endothelial ligand for $\alpha_L\beta_2$-integrin (LFA-1, Fig. S4). We, therefore, examined the role of endothelial JAM-A in the multistep immune cell migration pMBMECs in vitro. First, we confirmed apical accessibility of JAM-A in our inflamed BBB monolayer by performing live staining for JAM-A on pMBMECs stimulated with either IL-1β or TNF-α/IFN-γ, demonstrating luminal redistribution of JAM-A from the tight junctions to the apical side of the pMBMECs in the presence of the cytokines IL-1β or IFN-γ, where it can act as an adhesion molecule in our system (Fig. 5A). We next analyzed the migration of myelin-specific $CD4^+$ effector/memory T cells across JAM-$A^{-/-}$ and WT pMBMECs monolayers grown on filter inserts under static conditions. $CD4^+$ T cells migrated in similar numbers across unstimulated as well as TNF-α stimulated JAM-$A^{-/-}$ and WT pMBMEC monolayers (Fig. 5B). As shear forces impact on immune migration across endothelial monolayers, we next investigated the multistep $CD4^+$ T-cell migration across WT and JAM-$A^{-/-}$ pMBMECs under physiological flow by in vitro live cell imaging. We did not find a difference in the number of $CD4^+$ T cells arresting on WT and JAM-$A^{-/-}$ pMBMECs (Fig. 5C) under flow and neither in any postarrest dynamic T-cell behavior, such as T cell probing, crawling, diapedesis, or detaching (Fig. 5D). Moreover, the crawling velocity, distance, and directionality of continuously crawling T cells were indistinguishable on WT and JAM-$A^{-/-}$ pMBMECs (Fig. 5E–G). Thus, lack of JAM-A did not affect the multistep migration of T cells across the BBB in vitro.

Therefore, we next investigated the role of JAM-A in mediating the migration of macrophages across pMBMECs. As macrophages express JAM-A, we compared the interaction of JAM-$A^{-/-}$ unpolarized bone marrow-derived macrophages (BMDMs) with JAM-$A^{-/-}$ pMBMECs to that of WT BMDMs with WT pMBMECs under physiological flow in vitro. Although lack of JAM-A did not significantly affect the total number of BMDMs arresting to resting or stimulated pMBMECs and neither the percentage of extravasated or detached BMDMs (Fig. 5H–J), the postarrest behavior of BMDMs on IL-1β stimulated pMBMECs was altered in the absence of JAM-A (Fig. 5K). The percentage of BMDMs probing on the stimulated pMBMECs was significantly decreased,

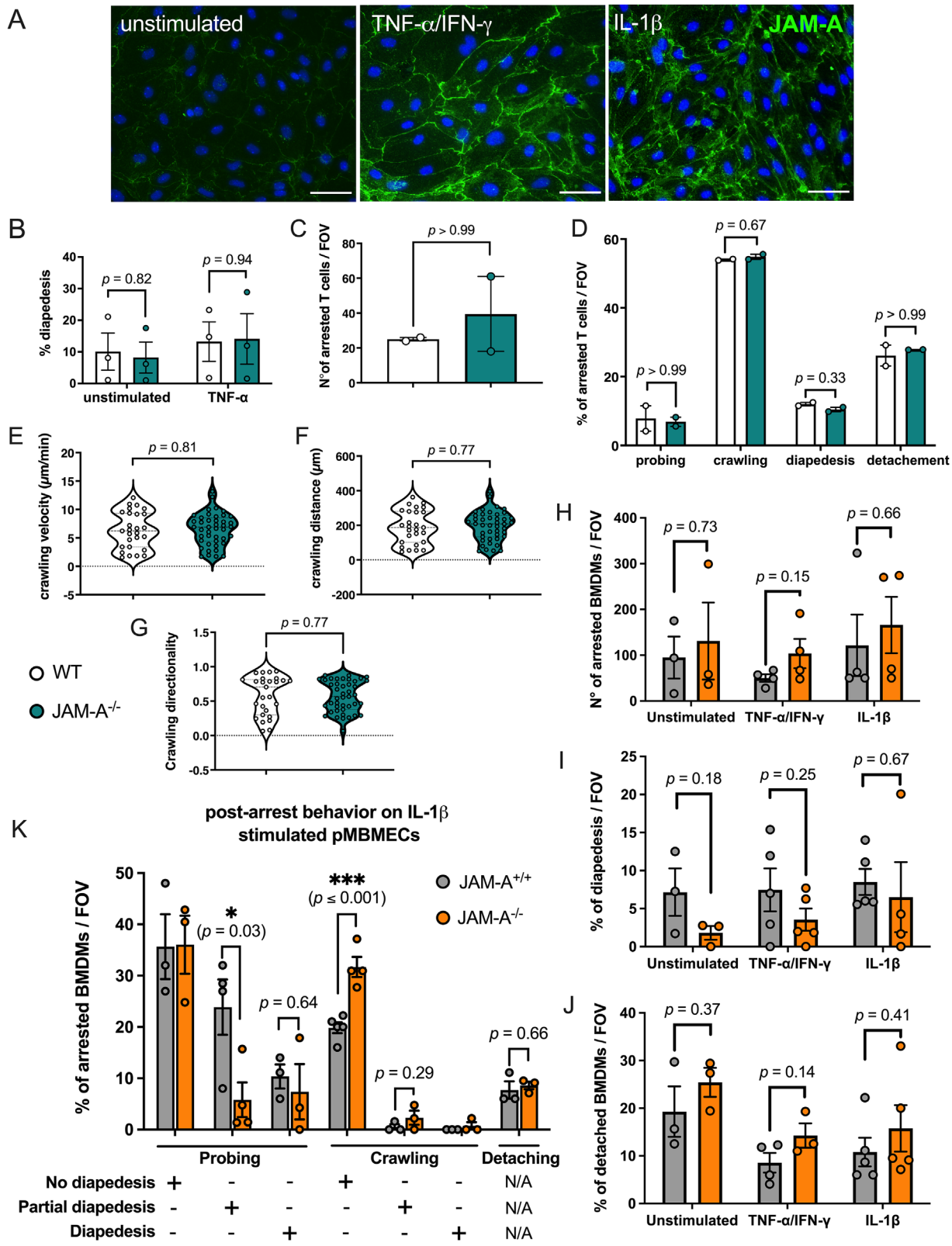

Figure 5. Lack of junctional adhesion molecule-A (JAM-A) affects the migratory behavior of macrophages on the highly inflamed blood–brain barrier (BBB) endothelium in vitro. (A) Cell surface immunofluorescence stainings for JAM-A (BV12) on alive unstimulated, tumor necrosis factor (TNF)-α + interferon (IFN)-γ or interleukin (IL)-1β stimulated primary mouse brain microvascular endothelial cells (pMBMECs) are shown. Scale bar: 50 μm. Images are representative of $N = 2$ independent experiments. (B) Diapedesis of encephalitogenic $CD4^+$ T cells across unstimulated or TNF-α treated confluent monolayers of wild type (WT) and JAM-$A^{-/-}$ pMBMECs under static conditions during 4 to 4.5 h. The percentage of transmigrated T cells was calculated from the input (1×10^5 T cells/well). ($N = 3$). (C and D) Analysis of the dynamic $CD4^+$ T-cell interactions with pMBMECs under

whereas the frequency of BMDMs continuously crawling with subsequent partial diapedesis (defined as an incomplete diapedesis event) was significantly increased. Of note, no differences in postarrest behavior of JAM-A$^{-/-}$ BMDMs were observed interacting with resting or TNF-α/IFN-γ stimulated pMBMECs (Fig. S5).

Taken together, our results suggest that while endothelial JAM-A is not essential for T-cell migration across the BBB in vitro, its expression on macrophages may play a more significant role in influencing the dynamic interactions observed between macrophages and the inflamed BBB. However, despite the influence of JAM-A on these interactions, its presence does not markedly alter the overall extravasation rate of BMDMs across the inflamed BBB in vitro.

Lack of JAM-A contributes to reduction of immune cell infiltrates into the CNS in vivo

After having observed a role for JAM-A in interaction of macrophages but not T cells with the BBB monolayer in vitro, we next explored if lack of JAM-A affects immune cell invasion into the CNS during aEAE in vivo with a focus on blood-borne macrophage infiltration. To this end, we crossed JAM-A$^{-/-}$ C57BL/6J mice with *CX3CR1*$^{+/GFP}$/*CCR2*$^{+/RFP}$ C57BL/6J mice [45] allowing to distinguish CNS-infiltrating CCR2^{+} monocyte-derived macrophages from CX3CR1^{+} CNS-resident myeloid cells based on their fluorescent reporter protein expression. We then went on to analyze different immune cell subsets in brain and spinal cord tissue from *JAM-A*$^{-/-}$*//CX3CR1*$^{+/GFP}$/*CCR2*$^{+/RFP}$ and *JAM-A*$^{+/+}$*//CX3CR1*$^{+/GFP}$/*CCR2*$^{+/RFP}$ mice at aEAE disease onset using quantitative flow cytometry (Fig. 6 and Fig. S6). The total counts of CD45^{+} inflammatory cells isolated from spinal cords (Fig. 6A,B) of *JAM-A*$^{-/-}$*//CX3CR1*$^{+/GFP}$/*CCR2*$^{+/RFP}$ were reduced when compared to their *JAM-A*$^{+/+}$ controls, whereas no marked differences could be detected in the amount of immune cell infiltrates into the brain tissues (Fig. 6C). Interestingly, quantification of different immune cell subsets revealed a significant reduction of CCR2^{+} macrophages and CD45^{high}CD11b^{neg} lymphocytes isolated from spinal cords of *JAM-A*$^{-/-}$*//CX3CR1*$^{+/GFP}$/*CCR2*$^{+/RFP}$ mice at aEAE disease onset (Fig. 6A,B) when compared to their *JAM-A*$^{+/+}$ controls. At the same time the number of brain infiltrating CCR2^{+} macrophages in *JAM-A*$^{-/-}$*//CX3CR1*$^{+/GFP}$/*CCR2*$^{+/RFP}$ mice was also slightly reduced compared to *JAM-A*$^{+/+}$ controls (Fig. 6C). In summary, these results highlight anatomical differences in the role of JAM-A in infiltration of immune cell subsets into the inflamed CNS, in which its absence affected immune cell entry into the spinal cord but not into the brain at onset of aEAE.

Given the presence of JAM-A on both microglia [46] and macrophages, and considering recent findings that highlight the role of microglial JAM-A in inhibiting their pathogenic phenotype in brain tumors [47], we investigated whether the absence of JAM-A influences the activation profile of these myeloid cells at EAE onset using flow cytometry. Interestingly, in the brain of *JAM-A*$^{-/-}$*//CX3CR1*$^{+/GFP}$/*CCR2*$^{+/RFP}$ mice suffering from aEAE, the percentage of MHC class II-positive microglia (Fig. S7B), but not macrophages (Fig. S7A), was consistently and strongly increased in four independent experiments along with a trend toward a higher proportion of MHC class II expressing microglia in the spinal cord. In contrast, other activation markers, including CD206, CD44, and CD86, were not significantly altered in CNS-infiltrating CCR2^{+} macrophages and CNS-resident CX3CR1^{high} microglia in the absence of JAM-A (Fig. S7).

Notably, we observed a consistent and marked increase in the percentage of MHC class II positive microglia in the brains of *JAM-A*$^{-/-}$*//CX3CR1*$^{+/GFP}$/*CCR2*$^{+/RFP}$ mice with aEAE across four independent experiments (Fig. S7B). This increase was specific to microglia, as macrophages did not show a similar trend (Fig. S7A). Additionally, a slight tendency toward a higher proportion of MHC class II expressing microglia was noted in the spinal cord. However, other activation markers, such as CD206, CD44, and CD86, did not exhibit significant changes in CNS-infiltrating CCR2^{+} macrophages and CNS-resident CX3CR1^{high} microglia in the absence of JAM-A (Fig. S7). These preliminary findings suggest a potential role for JAM-A in modulating microglial function in the brain. Nevertheless, further research is needed to establish a definitive link between the increased expression of MHC class II in microglia and the absence of JAM-A and to understand the functional implications of this observation.

Lack of JAM-A confines immune cells to CNS borders at onset of aEAE

JAM-A expression on astrocytes was previously shown to contribute to T-cell migration across the glia limitans into the CNS parenchyma [48]. This second step in immune cell migration

physiological flow of 1.5 dyn/cm^2 for 25 min, ($N = 2$). Each dot represents the average value of one experiment. (C) Number of arrested T cells per field of view (FOV) on TNF-α stimulated WT and JAM-A$^{-/-}$ pMBMECs. (D) Quantification of postarrest behavior of T cells with TNF-α stimulated WT and JAM-A$^{-/-}$ pMBMECs. The number of arrested T cells for each condition was set to 100% and the behavioral categories are shown as fraction thereof. (E–G) Violin plots of continuously crawling T cells on TNF-α stimulated WT and JAM-A$^{-/-}$ pMBMECs, tracked and analyzed for (E) crawling velocity, (F) distance, and (G) directionality (actual displacement divided by track length) ($N = 2$). Each dot represents one T cell. (H–J) Multistep migration of unpolarized bone marrow-derived macrophages (BMDMs) on either unstimulated, TNF-α + IFN-γ or IL-1β pMBMECs under physiological flow, ($N = 3$–5). Each dot represents the average value of one experiment. (H) Number of arrested BMDMs per field of view (FOV) ($N = 3$–4), (I) percentage of BMDMs undergoing complete diapedesis, (J) and the percentage of BMDMs detaching from WT and JAM-A$^{-/-}$ pMBMECs. (K) Quantification of postarrest behavior of BMDMs on IL-1β stimulated JAM-A$^{+/+}$ and JAM-A$^{-/-}$ pMBMECs. The number of arrested BMDMs for each condition was set to 100% and the behavioral categories are shown as fraction thereof. All datasets were analyzed using unpaired two-tailed students *t* test. Mean ± standard error of the mean (SEM) are shown. $^{*}p \leq 0.05$ and $^{***}p \leq 0.001$.

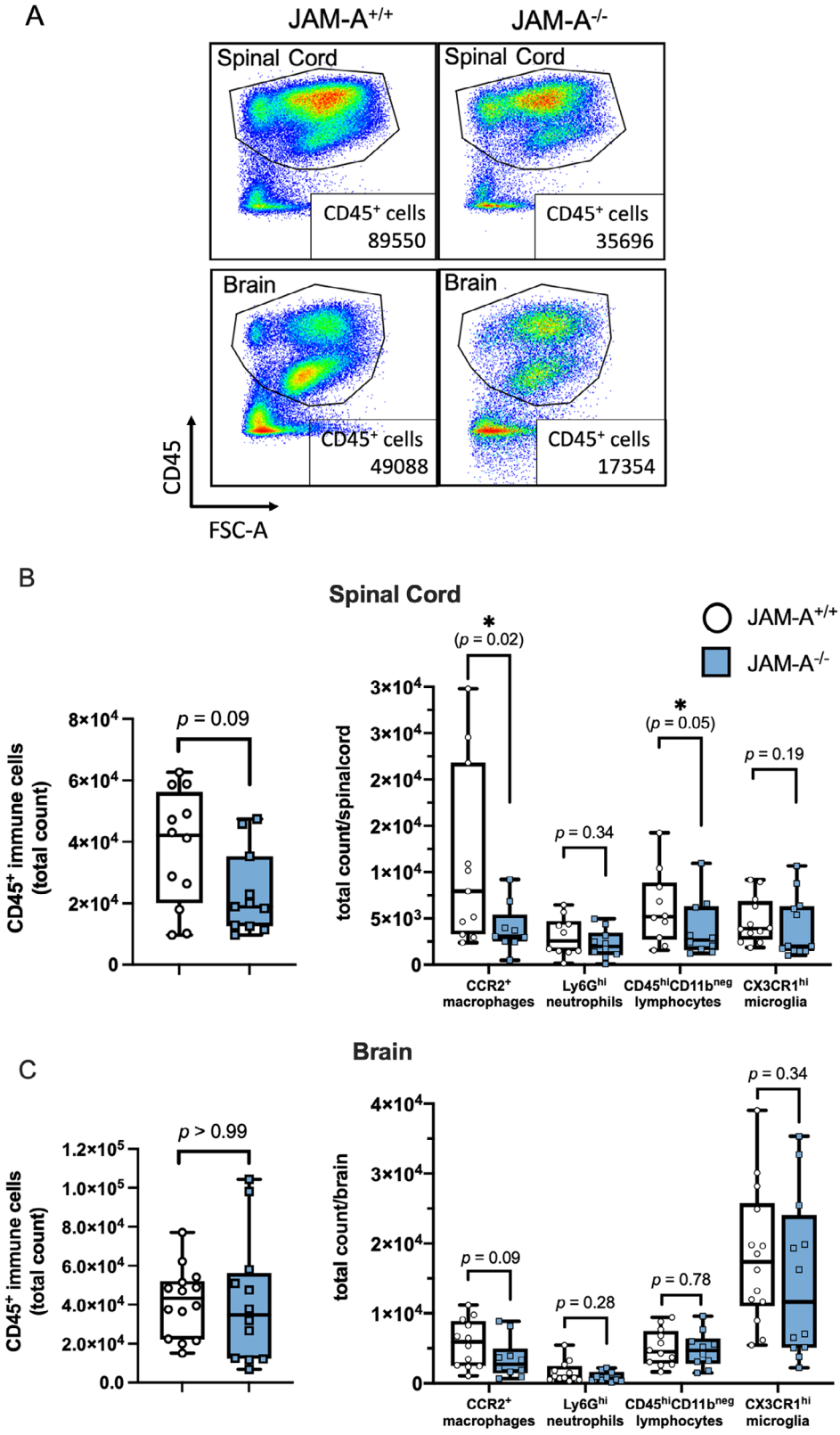

Figure 6. Lack of junctional adhesion molecule-A (JAM-A) reduces central nervous system (CNS) infiltration of CCR2$^+$ macrophages at active experimental autoimmune encephalomyelitis (aEAE) onset. (A) Gating strategy: Immune cells were defined based on their size (FSC) and CD45 positivity. Representative dot plots from flow cytometry analysis of CD45$^+$ immune cells isolated from spinal cords and brains of JAM-A$^{-/-}$ versus JAM-A$^{+/+}$ C57BL/6J mice at aEAE onset are shown. (B and C: left) Box-and-whisker plots representing the total number of CD45$^+$ immune cells isolated from (B) spinal cord and (C) brain of JAM-A$^{-/-}$ versus JAM-A$^{+/+}$ C57BL/6J mice at aEAE onset. (B and C: right) Absolute numbers of different CD45$^+$ immune cell subsets in (B) spinal cord and (C) brain. $N = 4$ independent experiments are shown in each graph; each square/dot represents one mouse. Box-and-whisker plots show median, 25%, and 75% percentile; lower/upper whisker lines end with the minimum/maximum value. Datasets were pooled across independent experiments and analyzed using unpaired two-tailed students *t* test. $^*p \leq 0.05$.

across the glia limitans into the CNS parenchyma is crucial for inducing clinial disease in EAE in C57BL/6J mice [49].

Therefore, we next asked if, in the absence of JAM-A, CNS infiltrating immune cells would remain confined to the CNS border compartments at aEAE onset. To this end, we performed immunofluorescence stainings using a pan-laminin antibody as a marker for endothelial and parenchymal basement membranes allowing to visualize the border compartments adjacent to the CNS parenchyma, namely, the PVS as well as the subarachnoid space. For quantification of macrophages, we made use of the *CX3CR1*$^{+/GFP}$*/CCR2*$^{+/RFP}$ reporter mice to distinguish CX3CR1^{+} resident microglia and border-associated macrophages from CCR2^{+} infiltrating macrophages, whereas CD3 staining served as a marker for T cells in cryosections of *JAM-A*$^{-/-}$*//CX3CR1*$^{+/GFP}$*/CCR2*$^{+/RFP}$ and *JAM-A*$^{+/+}$*//CX3CR1*$^{+/GFP}$*/CCR2*$^{+/RFP}$ mice at aEAE disease onset (Fig. 7). In accordance to our observations obtained by flow cytometry, the total number of CCR2^{+} infiltrating macrophages into the spinal cord parenchyma was significantly reduced, whereas more CCR2^{+} macrophages accumulated in the cerebral meninges in *JAM-A*$^{-/-}$*//CX3CR1*$^{+/GFP}$*/CCR2*$^{+/RFP}$ mice in comparison to *JAM-A*$^{+/+}$*//CX3CR1*$^{+/GFP}$*/CCR2*$^{+/RFP}$ mice (Fig. 7A). Similarly, in the absence of JAM-A, more CD3^{+} T cells were trapped in PVS of the spinal cord and in the meninges of the brain at aEAE disease onset (Fig. 7C).

Taken together, at aEAE onset lack of JAM-A leads to regional accumulation of CCR2^{+} macrophages and CD3^{+} T lymphocytes in CNS border compartments, which may ameliorate aEAE disease development.

Discussion

In the present study, we describe the contribution of the tight junction adhesion molecule JAM-A in the pathogenesis of aEAE, an animal model of MS. Lack of JAM-A resulted in amelioration of aEAE due to its contribution to immune cell infiltration into the CNS parenchyma and regional microglial activity.

In accordance with previous observations [17, 50], we here confirmed JAM-A expression in the cerebral microvasculature including the fenestrated endothelium of the ChP as well as the ChP epithelium. WT C57BL/6J mice suffering from aEAE showed increased numbers of JAM-A positive parenchymal vessels. Furthermore, intravenous injection of anti-JAM-A antibodies in WT mice with aEAE confirmed the redistribution of JAM-A from BBB tight junctions to the luminal side of the BBB endothelium during neuroinflammation. This focal redistribution of JAM-A to the endothelial surface has been described before in different in vitro and ex vivo studies using a variety of human endothelial cell lines [40, 41] or mouse BBB in vitro models in addition to peripheral vascular injury models [29, 39]. In line with a reorganization of vascular JAM-A during aEAE, alterations in the normally continuous JAM-A immunostaining of human cerebral vessels were also detected in brain tissue biopsies from patients with different forms of MS [34]. These studies showed discontinuous staining patterns for the tight junction molecules occludin, ZO-1, and JAM-A (but not of the adherens junction component β-catenin) in active and, to a lesser extent, in inactive MS lesions and normal appearing white matter [34–36, 51].

Importantly, JAM-A redistribution to the apical side of the endothelium during inflammation is believed to facilitate endothelial JAM-A *trans* homophilic or *trans* heterophilic interactions with JAM-A or LFA-1, respectively, with circulating immune cells and thereby promoting their migration across the endothelium [27]. In line with previous studies demonstrating expression of JAM-A also on different immune cell subsets [16, 19, 22, 52], we here confirmed cell surface expression of JAM-A on CD45^{+}CD11b^{+} myeloid cells while it was absent from mouse B and T cells. Thus, in the mouse, vascular JAM-A could engage homophilic and heterophilic adhesive interactions with myeloid cells, whereas T cells could only undergo heterophilic interactions with vascular JAM-A.

JAM-A expression was described on different structures in peripheral lymph nodes, including paracortical dendritic cells, sinus macrophages, lymphatic vessels, and high endothelial venules [22, 53]. In addition, JAM-A has been shown to impact on the random motility and directed migration of dendritic cells in secondary lymphoid tissues [22]. Thus, JAM-A could affect T-cell priming in response to $MOG_{aa35–55}$-immunization during induction of aEAE. However, in our present study, JAM-A$^{-/-}$ C57BL/6J mice did not show any defect in priming and activation of myelin-specific CD4^{+} T cells.

Given that previous studies have demonstrated a role for JAM-A in regulating paracellular permeability [20, 32], we explored its impact on BBB permeability using our well-established in vitro pMBMEC model, characterized by its high transendothelial electrical resistance and low permeability to small molecular tracers [42, 54]. Comparing the barrier properties of pMBEMCs from JAM-A$^{-/-}$ and WT C57BL/6J mice, we did not observe any significant role for JAM-A in maintaining BBB junctional integrity in vitro. This supports the previous notion that JAM-A may rather contribute to restoration of disrupted tight junctions than to the maintenance of tight junctional integrity in resting epithelial and endothelial cells [19, 20]. Alternatively, JAM-A was proposed to play a role in size selective and regional regulation of BBB integrity [55], as certain brain regions in JAM-A$^{-/-}$ mice showed enhanced permeability for the low molecular weight tracer sulpho-NHS-biotin (443 Da) and a slight but significant enhanced permeability for cadaverine (950 Da), whereas no vascular leakage was detected for 10 kDa dextran in mice with JAM-A deficiency [55]. Brain regions with enhanced vascular permeability correlated with a lower expression of claudin-5 in endothelial tight junctions, which was shown to be regulated by JAM-A via activation of the transcription factor CCAAT/enhancer-binding protein-α' (C/EBP-α) [55]. Our findings suggest that the absence of JAM-A and its reported contribution to a size-selective and regional increase in BBB permeability for molecules smaller than 1 kDa are negligible in light of the significant BBB breakdown characterizing EAE disease pathology.

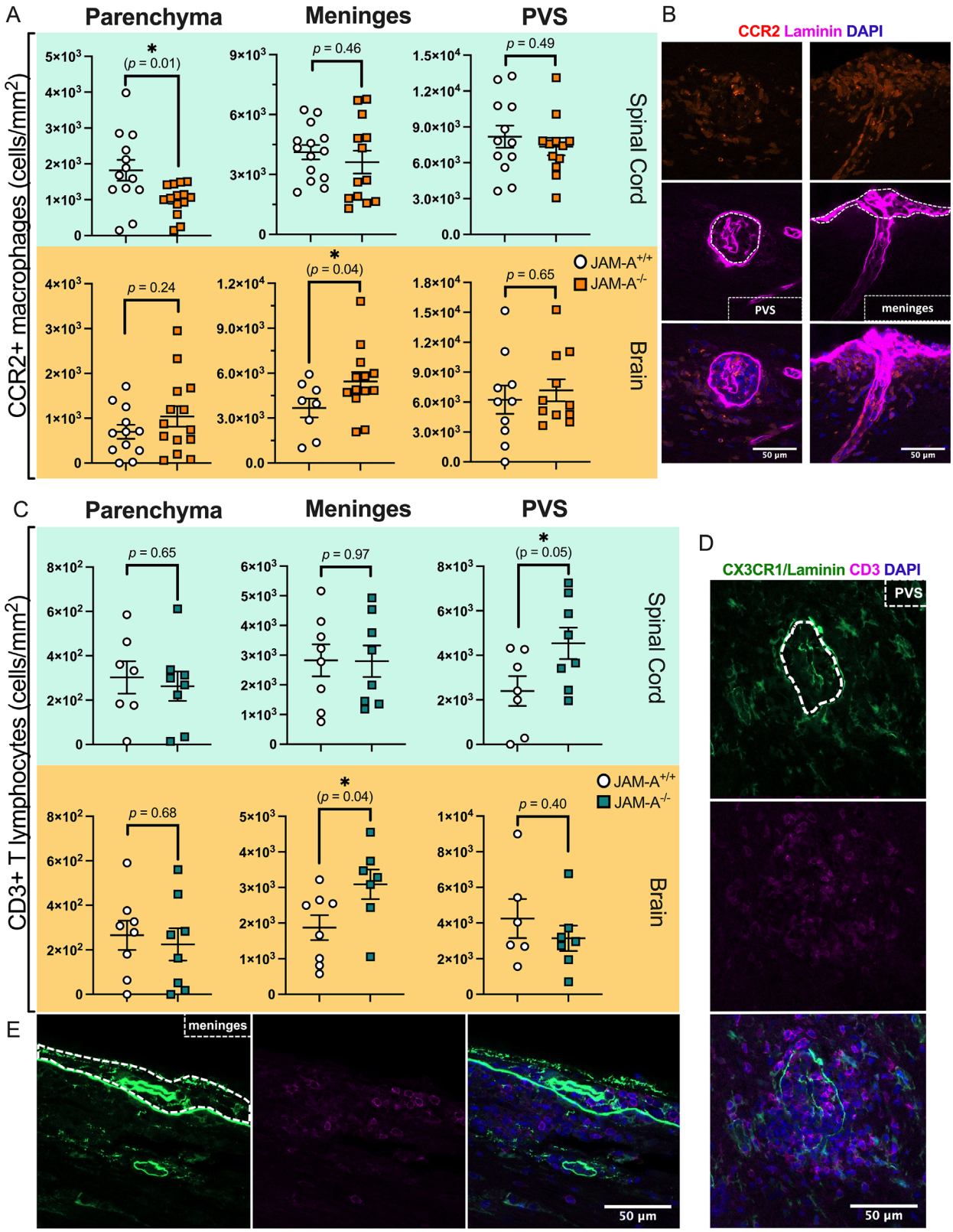

Figure 7. Lack of junctional adhesion molecule-A (JAM-A) reduces immune cell infiltration into the central nervous system (CNS) parenchyma at active experimental autoimmune encephalomyelitis (aEAE) onset. Quantification of CNS infiltrating CCR2$^+$ macrophages (A) and CD3$^+$ T cells (C) in 20 µm cryosections of brain and spinal cord from JAM-A$^{-/-}$ and JAM-A$^{+/+}$ C57BL/6J mice at aEAE onset (clinical score 0.5–1) is shown. Cells were assigned to the respective locations parenchyma, perivascular space (PVS), or meninges with respect to their positioning to the laminin positive endothelial and parenchymal basement membranes. From each mouse two sections per brain or spinal cord were analyzed and from each section

A function of JAM-A in limiting cell movement and migration has been previously established for dendritic cells, endothelial, and epithelial cell lines [22, 56, 57], and it has been shown that the knockdown or antibody blockade of endothelial JAM-A reduces the adhesion and transmigration of T cells across TNF-α treated human macro- and microvascular endothelial cells under static and flow conditions [27, 58]. In contrast, our observations show that lack of JAM-A does not affect the migration behavior and diapedesis of $CD4^+$ T cells across resting or TNF-α stimulated pMBMECs under static and physiological flow conditions. This observation is in line with previous studies from our laboratory, where we showed a predominant role of ICAM-1 and VCAM-1 in shear resistant arrest of encephalitogenic T cells to TNF-α stimulated pMBMECs, whereas crawling and subsequent diapedesis were mediated by ICAM-1 and ICAM-2 [42, 59]. The reason for those apparently discrepant results might be the utilization of Jurkat cells, an immortalized human T-cell line, as well as human $CD4^+CD45RO^+$ memory T cells, both known to express JAM-A [16, 19]. In contrast, mouse T cells do not express JAM-A as observed by us in the present study and others before [22]. As our studies furthermore showed that JAM-A is not a high affinity ligand for $CD4^+$ T cells, we conclude that rather JAM-A expressed by immune cells contributes to their interaction with endothelia either by *trans* homophilic binding to endothelial JAM-A or by influencing the interaction between endothelial JAM-A and leukocyte LFA-1. Interestingly, a similar mechanism was described for the interaction between endothelial JAM-B to VLA-4 ($\alpha_4\beta_1$-integrin), which was dependent on prior binding to JAM-C on T cells [60].

Furthermore, it was found that the involvement of JAM-A in neutrophil transmigration across the inflamed cremaster muscle vasculature is stimulus-dependent and only essential in the presence of IL-1β, whereas TNF-α cytokine stimulation bypassed the need for this adhesion molecule [61, 62]. In support of this notion, it was demonstrated that focal redistribution of JAM-A in human umbilical vein endothelial cells requires the stimulation of both TNF-α and IFN-γ [40]. This process of re-localization away from the tight junctional complex to the luminal side of the endothelium presents an integral step for JAM-A acquiring its role as a leukocyte adhesion molecule. It was furthermore reported that stimulation of the mouse brain endothelioma cell line bEnd.3 with CCL2 resulted in a prominent JAM-A redistribution to the apical surface accompanied by a strong increase in neutrophil and macrophage transmigration [29]. CCL2 is the strongest chemoattractant for monocyte/macrophage recruitment and implicated in inflammatory conditions dominated by monocyte-rich infiltrates [63]. Hence, considering the type of inflammatory stimulus and the reported role of JAM-A on certain immune cell subtypes, we next went on employing our live cell imaging setup on JAM-$A^{-/-}$ BMDMs interacting with either TNF-α/IFN-γ or IL-1β stimulated JAM-$A^{-/-}$ pMBMECs. Previous studies have shown that JAM-A is important for dynamic immune cell interactions with the endothelium, their polarized movement, as well as the subsequent diapedesis of monocytes and neutrophils at sites of inflammation [39, 64]. Consistent with these earlier findings, our current study reveals that BMDMs exhibit decreased probing and augmented crawling behavior on IL-1β stimulated pMBMECs when JAM-A is absent. Further underscoring a context-specific functions of JAM-A is a study that employed endothelial-specific JAM-$A^{-/-}$ mice as well as bone marrow chimeras with JAM-A-deficient immune cells in the context of atherosclerosis [39]. Immune cell-specific deficiency of JAM-A was achieved by reconstituting recipient mice after adaptive whole-body irradiation with bone marrow cells isolated from somatic JAM-$A^{-/-}$ mice [39, 65]. In this atherosclerosis mouse model, disturbed blood flow led to an increase and redistribution of JAM-A on the luminal surface, which in turn promoted plaque formation and monocyte infiltration. Interestingly, the absence of JAM-A in endothelial cells mitigated monocyte transmigration across the arterial wall, thereby attenuating inflammation. In contrast, the lack of JAM-A in bone marrow-derived immune cells exacerbated atherosclerotic lesions. This adverse effect was attributed to defective de-adhesion and incomplete transendothelial migration of JAM-A-deficient monocytes, resulting in their entrapment between the endothelial layer and the basement membrane, thereby inducing vascular damage. These findings underscore the context- and cell-dependent roles of JAM-A in different cell types within the vascular system. However, although lack of JAM-A affected the dynamic interaction of BMDMs on the BBB under flow in our in vitro model, this did not result in a significant reduction of BMDM diapedesis. In summary, our data revealed that JAM-A is not required in the multistep extravasation of $CD4^+$ T cells across the BBB in vitro. Concurrently, although JAM-A was involved in the dynamic engagement of macrophages with the BBB, its absence did not have a significant impact on their overall diapedesis across the BBB in vitro.

Despite the rather subtle involvement observed for JAM-A in the dynamic interaction of macrophages with the BBB in vitro, we went on to explore whether JAM-A contributes to immune cell migration across the BBB in vivo during aEAE. At aEAE onset, we found reduced numbers of $CCR2^+$ macrophages and $CD45^{high}CD11b^{neg}$ lymphocytes in the spinal cord in *JAM-*$A^{-/-}$*//CX3CR1*$^{+/GFP}$*/CCR2*$^{+/RFP}$ mice compared to their *JAM-*$A^{+/+}$*//CX3CR1*$^{+/GFP}$*/CCR2*$^{+/RFP}$ littermates. Thus, lack of JAM-A lead to reduced immune cell infiltration into the CNS in a regional and immune cell subset specific manner, resulting in

3–8 images were acquired for quantification and values were averaged for each CNS compartment/mouse. N = 3 (A) or N = 2 (C) independent experiments were performed. Mean ± standard error of the mean (SEM) are shown. Each dot/square represents one mouse. Datasets were pooled across independent experiments and analyzed using unpaired two-tailed students *t* test. Representative images (from JAM-$A^{-/-}$ mouse) of laminin bordered meninges and laminin bordered PVS in cerebellum (B) and cervical spinal cord (D and E) showing CNS-border compartments filled with and surrounded by infiltrating $CCR2^+$ macrophages and $CD3^+$ T lymphocytes, respectively. Scale bar: 50 µm.

amelioration of aEAE. This was accompanied by a focal increase in accumulation of immune cells in perivascular and meningeal spaces. In the C57BL/6J mouse immune cell, migration across the glia limitans into the CNS parenchyma is required to induce clinical signs of EAE [66, 67]. The observation of immune cell entrapment in leptomeningeal and PVS detected in *JAM-A*$^{-/-}$*//CX3CR1*$^{+/GFP}$*/CCR2*$^{+/RFP}$ mice parallels our earlier findings in JAM-B$^{-/-}$ C57BL/6J mice, which exhibited milder aEAE symptoms due to extensive trapping of infiltrating immune cells in CNS border compartments [68].

Interestingly, it was previously reported that reactive astrocytes can upregulate expression of the tight junctional molecules claudin-1, claudin-4, and JAM-A and form tight junctions between their aquaporin-4^{+} end-feet at the level of the glia limitans upon asymptomatic inflammatory focal lesion induction as well as in aEAE [48, 69]. Furthermore, as previously observed on endothelial cells, inflammatory stimuli release JAM-A from the astrocyte tight junctions, leading to a more dispersed cell surface expression and making JAM-A accessible for engagement by immune cells [48]. Mice lacking JAM-A specifically in astrocytes were observed to develop ameliorated aEAE by trapping T cells in PVS underscoring a role for JAM-A in mediating T-cell migration across the perivascular glia limitans [48]. Lack of JAM-A in astrocytes cocultured with T cells revealed a decrease of the inflammatory effector molecules such as CCL2, GM-CSF, and MMP-2, with proven roles in immune cell entry into the CNS parenchyma during EAE [48]. These previous data highlight the barrier function of the glia limitans in limiting T-cell infiltration into the CNS parenchyma and combined with our observations show that JAM-A mediates T-cell migration across the glia limitans rather than the BBB. Consistent with the findings of Amatruda et al., our observations also revealed an augmented accumulation of CD3^{+} T cells in the PVS of the spinal cord of EAE-afflicted mice associated with the absence of JAM-A. However, we did not concurrently observe a reduction in the presence of these cells within the CNS parenchyma. It is important to note, however, that the timing of our quantitative analysis differed to this previous study. While we conducted our analysis at the onset of EAE (13–15 days p.i.), Amatruda et al. focused on the peak of EAE (21 days p.i.). Considering the progressive increase in CNS immune cell infiltration during EAE, it is plausible that disparities in parenchymal CD3^{+} T-cell counts become more pronounced at later stages. This aspect certainly warrants further investigation. Building on the groundwork laid by Amatruda et al., our research broadens the scope to examine JAM-A functions in macrophage infiltration, assessing both in vitro and in vivo contexts. We specifically focused on the quantitative differences in the accumulation of monocyte-derived macrophages and T cells as they traverse various CNS barriers, notably the meninges and PVS, and drew comparisons between brain and spinal cord immune cell infiltrations. Notably, our observed regional and cell-specific variations in accumulation of these immune cell subtypes raises compelling questions, especially when juxtaposed with recent findings in the mouse and postmortem human brain tissue [70]. These findings identify a unique astrocyte population marked by myocilin expression, situated at the brain's glia limitans superficialis, displaying an unconventional anatomical arrangement with cell bodies at the surface and processes penetrating the parenchyma. Considering the crucial function of JAM-A expression in astrocyte end-feet, it is tempting to speculate that JAM-A is more accessible in the perivascular glia limitans than in the glia limitans of the CNS surface, thus mediating immune cell entry into the CNS in a region-specific manner. However, it is essential to acknowledge that the variation in CNS immune cell entry linked to the absence of JAM-A cannot be solely attributed to its role in astrocytes. Taken together, our data argue that JAM-A is not required for T-cell migration across the BBB but rather contributes to T-cell migration across the glia limitans during neuroinflammation. At the same time, JAM-A does contribute to macrophage interactions with the BBB, while its precise function in macrophage migration across this vascular barrier remains to be defined.

Beyond identifying a role of JAM-A in mediating immune cell entry into the CNS parenchyma, we made the surprising observation that in *JAM-A*$^{-/-}$*//CX3CR1*$^{+/GFP}$*/CCR2*$^{+/RFP}$ C57BL/6J mice suffering from aEAE, the expression levels of MHC class II on brain microglia were markedly enhanced. This suggests a role for JAM-A on microglial function during neuroinflammation, which was underscored by our observations of increased JAM-A immunostaining on microglial cells in close proximity to perivascular immune cell infiltrates during the onset of aEAE.

The mechanism by which an elevated abundance of MHC class II—expressing microglia in *JAM-A*$^{-/-}$ C57BL/6J mice may contribute to the alleviation of aEAE clinical symptoms is yet to be investigated. Existing research has indeed highlighted variations in the spatiotemporal engagement of microglial cells in the context of neuroinflammation. A protective CD11c^{+} microglia subpopulation was identified in aEAE and shown to reduce disease symptoms as well as demyelination when expanded upon administration with CSF-1 [71]. Notably, this subset of neuroprotective CD11c^{+} microglia expressed high levels of MHC class II and CD86, two surface molecules essential for antigen presentation [72]. Furthermore, in a mouse model for cuprizone-induced demyelination, the immunomodulatory function of MHC class II^{+} microglia was demonstrated, as mice lacking this molecule exhibited delayed remyelination and regeneration of oligodendrocytes [73]. Importantly, MHC class II expression is abundant on macrophages and microglia within demyelinated and remyelinated plaques in the brain of MS patients [74]. It is tempting to speculate that, via a yet unknown signaling pathway, JAM-A could be implicated in protective functions of activated (MHC class II^{+}) microglia during aEAE onset. This assumption is supported by another study in a mouse model for glioblastoma, in which lack of JAM-A changed the morphological and functional phenotype of microglia toward an anti-inflammatory and highly phagocytic state [47].

Finally, the role of JAM-A in mediating immune cell entry into the CNS via the ChP and blood-cerebrospinal fluid barrier should be considered. Both monocyte-derived macrophages and T cells have been suggested to enter the CNS parenchyma via the

ChP in certain pathological conditions [75–78]. In aEAE brains, we detected luminal accessible JAM-A on the fenestrated ChP endothelium, which could support the recruitment of circulating immune cells into the ChP stroma. Increased JAM-A immunostaining was also found on ChP epithelial cells, especially at their basolateral side. Previous studies have shown expression and upregulation of ICAM-1 and VCAM-1 on the apical side of ChP epithelial cells during aEAE [79, 80]. Thus, basolaterally expressed JAM-A may facilitate immune cell migration from the basolateral to the apical side of ChP epithelial cells, allowing for immune cell migration across the blood-cerebrospinal fluid barrier.

In summary, our study identified distinct roles for JAM-A in mediating immune cell entry into the CNS parenchyma during aEAE in addition to a role in microglial cell function in the brain.

Data limitations and perspective

Several limitations of our study warrant mention. First, our study relies on a constitutive JAM-A knockout mouse model, which does not allow for the dissection of cell-specific roles of this multifaceted molecule. The future use of cell-specific JAM-A knockout models will offer more refined understanding of its multifaceted roles, a notion supported by a growing body of research that emphasizes the varying functions of JAM-A across different inflammatory and tumoral settings [22, 39, 64, 81]. Second, the translational relevance of our findings to MS remains an open question, given that mouse T cells do not express JAM-A, unlike their human counterparts. As a result, our model may not completely recapitulate the mechanisms by which JAM-A may influence T-cell behavior in humans. Future studies should thus consider using human-derived BBB models, preferably in a coculture system that accurately represents the neurovascular unit, to enhance the translational relevance of the research. Finally, given that we observed luminal-accessible JAM-A on the fenestrated ChP endothelium, it would be valuable to explore the role of JAM-A in mediating immune cell entry into the CNS via the ChP.

Materials and methods

Mice

The generation and genotyping of *JAM-A*$^{-/-}$ mice on a unibJ background was described previously [22]. JAM-A$^{-/-}$ C57BL/6J mice were crossed with a *CX3CR1*$^{+/GFP}$/*CCR2*$^{+/RFP}$ C57BL/6J reporter mouse line kindly provided by Dr. Israel F. Charo (UCSF) and described previously [45]. Mice were housed under specific pathogen free conditions in individually ventilated cages. Only female mice between 6 and 12 weeks were used for experiments. Note that Fig. 5H–K, 6 and 7 as well as Fig. S5–S7 refer to JAM-A$^{-/-}$ C57BL/6J mice crossed with the reporter mouse line *CX3CR1*$^{+/GFP}$/*CCR2*$^{+/RFP}$ C57BL/6J.

Induction of active EAE

aEAE was induced in JAM-A$^{-/-}$ C57BL/6J mice and WT littermates by subcutaneous injection of 200 μg of myelin oligodendrocyte glycoprotein peptide ($MOG_{aa35-55}$) in 100 μL of complete Freund's adjuvant (incomplete Freund's adjuvant (Santa Cruz) supplemented with 4 mg/mL nonviable, desiccated *Mycobacterium tuberculosis* (H37 RA, DIFCO Laboratories, Detroit, MI; CFA) into 8–12 weeks old female mice as described before [82]. 300 ng pertussis toxin from Bordetella pertussis (LuBioScience GmbH) per mouse was administered intraperitoneally at days 0 and 2 p.i. Assessment of clinical disease activity was performed as described before [82] with the following disease scores: 0 = asymptomatic, 0.5 = limp tail, 1 = hind leg weakness, 2 = hind leg paraplegia, and 3 = loss of lower body control and incontinence.

Detection of luminal JAM-A in WT C57BL/6J mice

Endotoxin-free rat anti-mouse JAM-A (BV12), rat anti-mouse PECAM-1, and rat anti-human CD44 (used as isotype control) antibodies for in vivo use were purified from serum-free hybridoma culture supernatants. Per mouse 100 μg of the respective antibody (60–90 μL) was injected into the tail vein and allowed to circulate for 15–20 min. Mice were deeply anaesthetized with isoflurane and perfused with 10 mL cold phosphate buffered saline (PBS) followed by 10 mL of 1 % paraformaldehyde (PFA) in PBS.

Isolation of primary mouse brain microvascular endothelial cells (pMBMECs)

pMBMECs from the cortex of female 6 to 8 weeks old JAM-A$^{-/-}$ C57BL/6J and WT C57BL/6J or *JAM-A*$^{-/-}$*//CX3CR1*$^{+/GFP}$/*CCR2*$^{+/RFP}$ C57BL/6J and *JAM-A*$^{+/+}$*//CX3CR1*$^{+/GFP}$/*CCR2*$^{+/RFP}$ C57BL/6J mice were isolated and cultured exactly as previously described [54, 83].

Isolation of T cells

For static transmigration assays, proteolipid protein (PLP)-specific effector/memory CD4^{+} Th1 cells [84] were used at 3–7 days after restimulation with the PLP peptide (aa139-151) antigen. T lymphocytes for live cell imaging were isolated from the spleen of a C57BL/6J WT mouse via negative selection (Dynal Mouse T cell Negative Isolation Kit, Invitrogen) and activated for 24–48 h with rat anti-mouse CD3 and rat anti-mouse CD28 antibodies (both at 0.1 μg/mL, Pharmingen BD Biosciences). The purity of these T cells was determined by flow cytometry for CD90.2 (Thy1.2) at the day of the experiment and was always above 90%.

Isolation of bone marrow-derived macrophages

BMDMs were harvested from pelvis, femur, and tibia bones of female 6 to 14 weeks old *JAM-A*$^{-/-}$*//CX3CR1*$^{+/GFP}$*/CCR2*$^{+/RFP}$ C57BL/6J and *JAM-A*$^{+/+}$*// CX3CR1*$^{+/GFP}$*/CCR2*$^{+/RFP}$ C57BL/6J mice. Under sterile conditions, the bone marrow was flushed out using BMDM medium (RPMI with glutamine Gibco) supplemented with 10 % heat-inactivated fetal bovine serum (FBS, Gibco) and 100 U/mL penicillin–streptomycin (Gibco). Following the filtration through a 100 μm nylon mesh, bone marrow cells were washed by adding 20 mL of BMDM medium followed by centrifugation at 280 g for 5 min at 4°C. Erythrocytes were depleted by incubation with ACK lysis buffer (Gibco) for 5 min on ice. Cell lysis was stopped by adding 20 mL of BMDM medium and cells were washed again. Bone marrow cells were plated in a density of 17–20 $\times$ 10^6 cells/mL in BMDM medium supplemented with 5 ng/mL of recombinant mouse macrophage colony stimulating factor (mCSF, R&D Biosystems 416-ML-500) onto non-treated 100 mm tissue culture petri dishes (Greiner Bio-One) and cultured for 7 days at 37°C and 5% CO_2. BMDM media containing macrophage colony stimulating factor was changed every 3–4 days and differentiated macrophages harvested by incubation with 0.05% Trypsin (Gibco, 25300-054) for 10 min at 37°C.

In vitro live cell imaging under physiological flow conditions

In vitro live cell imaging was performed on pMBMEC monolayers cultured on Matrigel-coated (Corning) μ-dishes (35 mm low, ibidi) with a custom-made flow chamber mounted onto the ibidi dishes as previously described [85]. Ibidi dishes were placed on a stage of an inverted microscope (AxioObserver, Carl Zeiss) equipped with a temperature-controlled 37°C chamber as previously described. T cells or BMDMs were resuspended in migration assay medium (MAM (Dulbecco's modified eagle medium (DMEM, Gibco), 5% FBS, 4 mM L-glutamine (Gibco, A2916801) and 25 mM HEPES buffer solution (Gibco, 15630-056). To study the interaction with pMBMECs under flow, a total of 5 $\times$ 10^5 T cells or 2.5 $\times$ 10^5 BMDMs/experiment were perfused over the pMBMEC monolayers.

Immune cells were allowed to accumulate on the pMBMECs for 4 min (T cells) or 5 min (BMDMs) at low shear stress (0.25 dyn/cm^2). Next, medium flow was increased to physiological shear stress (1.5 dyn/cm^2) and dynamic T cell or BMDM interaction with pMBMECs was continued to be recorded for a total of 30 min (including accumulation phase) taking 1 frame/10 s. Videos were acquired with phase contrast and a 10$\times$ objective. The time-lapse videos were analyzed using ImageJ software (National Institutes of Health). Analysis of cell numbers and migratory behavior was started 30 safter the start of physiological shear flow using ImageJ. Postarrest behavior of immune cells on the endothelium was divided into four categories: 1. "probing" defined as an immune cell remaining at the same position after arrest and extending its protrusions into the surroundings, 2. "crawling" on the surface of the endothelial monolayer defined as cell displacement of more than one cell diameter, 3. "diapedesis" of an immune cell migrating through the endothelium (with prior probing or crawling), and 4. "detachment" of a cell from the endothelium during the observation period as previously described [42, 85]. The additional subcategory "partial diapedesis" was employed for postarrest behavior of BMDMs defined as a cell starting diapedesis and sending protrusions underneath the endothelial monolayer without complete transmigration during the observation period. Crawling speed, directionality, and distance of T cells were analyzed using the chemotaxis and migration tool plugin in ImageJ [86].

T-cell diapedesis under static conditions

Static T-cell diapedesis assays were carried out as described before [87, 88]. In brief, pMBMECs were cultured in a two-chamber system on Transwell filter inserts with 5 μm pore size (Corning Costar Corporation) until confluence. Per well, 1 $\times$ 10^5 T lymphocytes were added to the upper chamber and allowed to transmigrate across the endothelial monolayer for 4–4.5 h in the incubator. Assays were performed in triplicates for each preparation/condition.

T-cell proliferation assay

In vitro antigen-recall assays were carried out with $MOG_{aa35–55}$-immunized JAM-A$^{-/-}$ C57BL/6J and WT C57BL/6J mice exactly as described before [89]. Increasing concentrations of $MOG_{aa35–55}$ and 10 μg/mL of purified protein derivate of *M. tuberculosis* (PPD, CFA-component) were used to test for antigen-specific T-cell proliferation. T-cell proliferation induced by the mitogen ConA (2.5 μg/mL) or by cross-linking of CD3 and CD28 with 0.1 μg/mL of the respective antibodies (Pharmingen BD Biosciences) was used as positive control.

In vitro binding assay under static conditions

Binding assay with recombinant adhesion molecules was performed as previously described [90]. In brief, Teflon slides were coated with recombinant proteins (recombinant DNER-Fc chimera 100 nM, R&D 2254-DN; recombinant ICAM-1-Fc chimera 100 nM, R&D 796-IC; or recombinant JAM-A-Fc chimera either at 25, 50, 100, or 200 nM, R&D 1077-JM) for 2 h at 37°C. PLP-specific CD4$^+$ T_H1 effector/memory T cells [84] were collected in assay medium (DMEM, HEPES 25 mM, 5% calf serum, 2% L-glutamine) at a concentration of 1 $\times$ 10^7 cells/mL. A volume of20 μL cell suspension (2 $\times$ 10^5 cells/field) was added to the coated slides and incubated for 30 min on a rotating platform at room temperature. Diagnostic microscopy slides were washed and fixed with 2.5% (v/v) glutaraldehyde in PBS. Analysis was

performed by counting the cells bound per field of view under the microscope using a grid ocular.

Permeability of pMBMEC monolayers

In vitro permeability of the pMBMEC monolayers was assessed by measuring the clearance of Alexa Fluor 680-labeled 3 or 10 kDa dextran (Thermo Fisher Scientific) exactly as described before [91, 92]. In brief, the fluorescent tracers diffusing across the pMBMEC monolayers were collected from the bottom well every 20 min for a total of 60 min. Fluorescence intensity for Alexa Fluor 680-labeled dextrans was measured by infrared imaging (Odyssey Quantitative Fluorescence Imaging System, LI-COR). The endothelial permeability coefficient (Pe) was calculated as previously described [93]. The experiments were performed in triplicates for each condition.

Isolation of brains and spinal cords from JAM-A$^{-/-}$ and WT C57BL/6J mice and tissue processing

Mice were sacrificed with an overdose of isoflurane (Baxter, Arovet AG) and perfused with PBS through the left ventricle of the heart. Brains and spinal cords were dissected, embedded in Tissue-Tek (OCT compound, Sysmex Digitana AG), and snap frozen in a dry ice/isopentane bath (Grogg Chemie AG). Thick cryosections of 6 μm were prepared and air-dried overnight.

Isolation of skulls and vertebrae columns from *JAM-A$^{-/-}$//CX3CR1$^{+/GFP}$/CCR2$^{+/RFP}$* and *JAM-A$^{+/+}$//CX3CR1$^{+/GFP}$/CCR2$^{+/RFP}$* mice and tissue processing

Mice were sacrificed with an overdose of isoflurane and transcardially perfused first with 10 mL of ice-cold PBS followed by 10 mL of cold 4% PFA/PBS. Whole skull and vertebrae column were harvested and stored overnight in 4% PFA/PBS at 4°C. Following a wash with PBS, tissue samples were stored in 14% EDTA (Sigma Aldrich, Cat. E5135, in distilled water adjusted to pH 7.8–8) for 7 days while renewing the EDTA solution every second day [94]. After decalcification of the bones, samples were washed again and stored in 30% sucrose/PBS for 3 days, washed with PBS, embedded in Tissue-Tek, and frozen in a dry ice/isopentane bath. Cryosections of 20 μm were prepared and air-dried overnight.

Immunohistochemistry

Cryosections of 6 μm cryosections were fixed in acetone at −20°C for 10 min and immuno-stained using a three strep immunoperoxidase technique and hematoxylin counterstain exactly as described before [95].

Immunofluorescence stainings

Brain cryosections

For immunofluorescence staining of tissue sections, acetone-fixed frozen sections were blocked for 20 min with 5% (w/v) skimmed milk, 0.3% (v/v) Triton X-100, and 0.04% (w/v) NaN_3 in TBS (blocking buffer), washed with PBS, and incubated for 1 h each with primary and secondary antibodies (Tables 1 and 2) diluted in blocking buffer. After a final PBS wash, sections were mounted in Mowiol (Calbiochem, Grogg Chemie AG).

Decalcified skull and vertebral column cryosections

Cryosections were permeabilized with 0.1% TritonX-100 (Fluka via Grogg Chemie AG, Switzerland) in PBS for 10 min and blocked with 10% normal goat serum or 5% BSA in PBS for 1 h at RT. Incubation with primary antibodies (rabbit anti-mouse laminin 1 + 2, rat anti-mouse CD3) diluted in 3% goat serum/PBS was performed overnight at 4°C. Cryosections were washed with PBS prior to incubation with secondary antibodies (goat anti-rabbit Alexa Fluor 647, goat anti rabbit Alexa Fluor 488, and donkey anti rat Cy5) diluted in 3 % normal goat serum/PBS applied for 2 h at RT. Sections were washed with PBS and nuclei stained with DAPI for 15 min at RT. After a final PBS washing step, slides were mounted in Mowiol.

Fixed pMBMECs

For immunofluorescent staining of claudin-5, ZO-1, JAM-A, VCAM-1, and occludin on pMBMECs, cells were grown on 8-well Lab Tek chamber slides (Milian SA) to confluency and fixed with either ethanol at 4°C for 10 min, with 1% PFA/PBS at room temperature for 10 min or with ice-cold methanol for 30 s, respectively. All further steps were performed at room temperature. Blocking was performed with blocking buffer for 20 min. Both primary and secondary antibodies were diluted in the same blocking solution and incubated for 1 h each, with TBS washing steps in between, followed by nucleus staining with DAPI for 2 min. After a final wash, chamber slides were mounted in Mowiol.

Live pMBMECs

For staining live pMBMEC for JAM-A, pMBMECs were seeded onto a Matrigel-coated 12-well silicon chamber with a 0.56 cm^2 surface area/well. On day 6 pMBMECs were stimulated with either 20 ng/mL of recombinant murine IL-1β, 5 ng/mL of recombinant murine TNF-α or 100 IU/mL IFN-γ + 5 ng/mL TNF-α for 16–20 h. Live pMBMEC monolayers were incubated with rat anti-mouse JAM-A (BV11) for 13 min at RT. Cells were then fixed with 1% PFA/PBS for 10 min, washed twice with PBS, and incubated with

Table 1. Primary antibodies used for immunofluorescence/immunohistochemistry.

Antibody	Clone	Provider	Catalogue N° reference	Isotype
Rat anti-mouse JAM-A	BV12	E. Dejana, Milan, Italy [97]	Hybridoma culture supernatant	IgG2b or IgG2a
Rabbit anti-mouse JAM-B	αJB829	B. Imhof, Geneva, Switzerland [98]		Rabbit IgG2a
Rabbit anti-mouse JAM-C	polyclonal	[99]		Rabbit IgG
Rat anti-mouse CD45	M1/9	Made in-house	Hybridoma culture supernatant	Rat IgG2a
Rat anti-mouse VCAM-1	9DB3	Made in-house [100]	Hybridoma culture supernatant	Rat IgG2a
Rat anti-human CD44	9B5			Rat IgG2a
Rabbit anti-mouse ZO-1	Polyclonal	Zymed, San Francisco, USA via LuBioScience GmbH, Switzerland	61-7300	Rabbit IgG
Rabbit anti-mouse occludin	Polyclonal	Invitrogen	71-1500	Rabbit IgG
Rabbit anti-mouse claudin-5	Polyclonal	Zymed via LuBioScience GmbH, Switzerland	34-1600	Rabbit IgG
Rabbit anti-mouse laminin 1+2	Polyclonal	Abcam	ab7463	Rabbit IgG
Rat anti-mouse PECAM-1	Mec13.3	Made in-house [101]	Hybridoma culture supernatant	Rat IgG2a
Goat anti-mouse Iba1	Polyclonal	Abcam	Ab5076	IgG
Rabbit anti-mouse IgG control	Polyclonal	R&D systems	AB-105-C	Rabbit IgG
Rat anti-mouse CD3	KT3	AbD Serotec	MCA500G	Rat IgG2a

Abbreviation: JAM, junctional adhesion molecule.

secondary antibody (donkey anti-rat AlexaFluor 488) diluted in 5% (w/v) skimmed milk in PBS for 45 min at RT. pMBMECs were washed again, nuclei stained with DAPI for 5 min at RT, and slides mounted in Mowiol.

Spatial quantification of CNS infiltrating immune cells in decalcified skull and vertebral column cryosections

For analysis of CNS infiltrated CCR2$^+$ macrophages and CD3$^+$ T-cell numbers in certain CNS sub-compartments of 20 μm decalcified skull and vertebrae column cryosections from *JAM-A*$^{-/-}$*//CX3CR1*$^{+/GFP}$*//CCR2*$^{+/RFP}$ and *JAM-A*$^{+/+}$*//CX3CR1*$^{+/GFP}$*//CCR2*$^{+/RFP}$ mice, the following procedure was employed: Cryosections were stained with either a pan-laminin marker alone or together with rat anti-mouse CD3 antibody (as described above) in order to visualize RFP$^+$ (CCR2) macrophages and Cy5$^+$ (CD3) T lymphocytes within laminin + endothelial and parenchymal basement membranes of PVS and meninges. Z-stack images of 20 μm decalcified skull and vertebral column cryosections with 0.5 μm intervals were acquired using a confocal microscope (LSM800, Zeiss) with a 25× objective. From each z-stack, one plane with a visually clear delineation of the laminin + basement membranes was selected for further analysis. Image acquisition settings were kept consistent for all images. QuPath (v.0.3.2) was used for data analysis Github, (https://QuPath.github.io/). Regions of interest (CNS parenchyma, PVS, and meninges) were identified based on their laminin positivity as a marker for endothelial + parenchymal basement membranes and annotated manually in every image using the "brush" tool. First, all cells were segmented by DAPI$^+$ nuclei identification using the "cell detection" function while carefully adjusting for the following parameters to ensure accurate cell nuclei detection: pixel size, background radius, median radius, sigma, minimum area, maximum area, and threshold of cell nuclei. After parameter setup, the accuracy of automated

Table 2. Secondary antibodies used for immunofluorescence stainings.

Antibody	Conjugate	Provider	Cat. No
Donkey anti-goat IgG	Cy3	Jackson immunoresearch	AB_2307351
Goat anti-rabbit IgG	Cy3	Jackson immunoresearch	AB_2307443
Goat anti-rat IgG	Cy3	Jackson immunoresearch	AB_2340667
Donkey anti-rat IgG	Alexa Fluor 488	Jackson immunoresearch	AB_2340683
Goat anti-rabbit IgG	Alexa Fluor 488	LubioScience	111-545-003
Goat anti-rat IgG	Alexa Fluor 488	LubioScience	112-545-003
Goat anti-rabbit IgG	Alexa Fluor 647	ThermoFisher Scientific	A32733
Donkey anti-rat	Cy5	Jackson immunoresearch	712-175-153

cell detection was verified by comparing cell counts to manual cell counts of two blinded researchers in a first pilot experiment. After optimization of cell detection parameters, the cell class for RFP^+ (CCR2) macrophages or $Cy5^+$ (CD3) T cells was defined by optimizing the intensity threshold parameter for RFP (thresholds between 5 and 40 were tested in increments of 5) or Cy5 (thresholds between 100 and 300 were tested in increments of 20) signal intensity, respectively. The threshold parameter was measured as mean value in the RFP^+ or $Cy5^+$ macrophage or T cell, respectively. Accurate threshold parameter setup for detection of RFP^+ and $Cy5^+$ cells was ensured by comparison to manual counts with visual inspection in a first set of experiments by two blinded researchers.

Parameters were set up separately for brain and spinal cord in order to accommodate the need for different color thresholds in different tissues. On the basis of the optimized cell detection and classification setup a script was generated in QuPath allowing an automated cell quantification after manual region annotation for the whole project. Measurements of cell counts and area of annotations were exported using the Measurement Exporter in QuPath and calculated for each region of interest as cells/mm^2.

From each mouse two cryosections per CNS tissue (i.e., brain and spinal cord) were analyzed and from each cryosection 3–8 images were acquired for quantification. Values were averaged to aquire one value per CNS compartment (i.e., meninges, PVS, and parenchyma) in brain or spinal cord per mouse. Three (macrophages) or two (T cells) independent experiments were performed with mice at aEAE onset (score 0.5–1).

Isolation of immune cells from brains and spinal cords

Brain and spinal cord were processed separately for flow cytometry analysis. The tissue was cut into fine pieces within a 100 mm petri dish filled with 1 mL of digestion medium (0.4 mg/mL Collagenase VIII (Sigma, C2139) and 2 U/mL DNAse (Roche) in HBSS ($MgCl^+$ $CaCl^+$, Gibco) and incubated at 37°C in a shaking water bath for 30 min. Digestion was stopped by adding 20 mL of FACS buffer (2% FCS (SeraGlob S11500 in PBS) and centrifuged for 2 min at 280 *g* at 4°C and the supernatant was discarded. Tissue was transferred into a Wheaton Glass Tissue Grinder containing dissection medium (1.5% 1M HEPES, 1.3% glucose solution in HBSS) and carefully homogenized. The homogenates were filtered through a 70 μm cell strainer, centrifuged for 10 min at 280 *g* at 4°C and the cell pellets resuspended in 10 mL of 37% Percoll (Ge Healthcare Biosciences, 17-0891-01) and centrifuged for 30 min and 600 *g* at 4°C without a deceleration break. This step allows the separation of immune cells from myelin debris and red blood cells by creating a Percoll density gradient with a myelin ring and cell debris forming at the top and a blood cell ring at the bottom. Th cell fraction enriched for $CD45^+$ leukocytes was collected right underneath the myelin ring and transferred to a new tube and filtered through a 70 μm cell strainer. The single cell suspension was washed twice with FACS buffer by centrifugation for 5 min at 280 *g* and 4°C and prepared for antibody staining.

Flow cytometry analysis of CNS immune cells during aEAE onset

For this step the single-cell suspension was first incubated with anti-CD16/32 antibody for 15 min on ice to block Fc receptors and therefore reduce unspecific antibody binding. After a wash with FACS buffer (2% FCS in PBS) and 5 min of centrifugation at 4°C and 280 *g* the cell suspension was incubated for 30 min on ice with respective antibodies (Table 3). Compensation controls included unstained cells serving as negative control as well as single-color stains positive for each fluorophore used. Samples were acquired using an Attune NxT cytometer (Thermo Fisher Scientific). For data analysis, the software FlowJo was used (Version 10).

For analysis of different immune cell subsets in the inflamed CNS of mice at aEAE onset, the following gating strategy was employed (Fig. S8): First, cells were identified based on size and granularity (FSC-A vs. SCC-A) and doublets excluded via a FSC-H and FSC-A density plot. Dead cells were gated out based on their eFluor506 viability dye positivity. After gating on $CD45^+$ leukocytes (CD45 vs. FSC-A), a CD45 versus CD11b gate was plotted to distinguish $CD45^{high}$ $CD11b^{negative}$ lymphocytes, $CD45^{interm}CD11b^{interm}$ CNS-resident macrophages, and $CD45^{high}CD11b^{high}$ blood–borne infiltrating myeloid cells. From the $CD45^{interm}CD11b^{interm}$ population, $CD45^{interm}CD11b^{interm}CX3CR1^{high}$ microglia were identified. Within the $CD45^{high}CD11b^{high}$ myeloid cell population, $CD45^{high}CD11b^{high}Ly6G^{high}Ly6C^+$ neutrophils and $CD45^{high}$ $CD11b^{high}Ly6C^{high}Ly6G^{low}$ macrophages were selected. From the latter cell population, $CD45^{high}CD11b^{high}Ly6C^{high}Ly6G^{low}CCR2^+$ infiltrating macrophages were identified. Within the $CD45^{interm}$ $CD11b^{interm}CX3CR1^{high}$ and $CD45^{high}CD11b^{high}Ly6C^{high}Ly6G^{low}$ $CCR2^+$ myeloid cell populations, respectively, the expression of MHCII, CD44, CD86, and CD206 was analyzed. As a readout for these functional markers, the percentage of positive cells (MHCII, CD206, and CD86) as well as the relative median fluorescence intensity (CD44) were calculated.

Statistics

All statistical analyzes were performed using Graph Pad Prism 9.0 software (La Jolla). Data are presented as mean ± standard error of mean, mean ± standard deviation, or box-and whisker plots as indicated in the respective figure legends. Datasets were first tested for normal distribution using Shapiro–Wilk normality test followed by unpaired students *t* test. When datasets were not normally distributed a nonparametric Mann–Whitney *U* test was performed. For better visualization of data variability and reproducibility, a color-coded Superplot [96] was employed in Fig. 3B, superimposing average statistics (paired two-tailed *t* test) derived from repeated experiments onto a graph encompassing all biological replicates per experimental group. Asterisks indicate significant differences ($*p \leq 0.05$; $**p \leq 0.01$; $***p \leq 0.001$).

Table 3. Antibodies used in flow cytometry panels.

Antibody	Fluorophore	Clone	Provider	Cat. No	Isotype
Rat anti-mouse CD11b	PerCP	M1/70	BioLegend	101230	Rat IgG2b
Rat anti-mouse CD45	Alexa Fluor 700	30-F11	BioLegend	103128	Rat IgG2b
Mouse anti-mouse CD45	Qdot800	HI30	ThermoFisher Scientific	Q10156	Mouse IgG1
Rat anti-mouse MHC class II	BV421	M5/114.15.2	BioLegend	107631	Rat IgG2b
Rat anti-mouse MHC class II	Pacific Blue	M5/114.15.2	BioLegend	107620	Rat IgG2b
Rat anti-mouse Ly6C	APC-Fire750	HK1.4	BioLegend	128046	Rat IgG2c
Rat anti-mouse Ly6C	Alexa Fluor 700	HK1.4	BioLegend	128024	Rat IgG2c
Rat anti-mouse CD44	BV605	IM7	BioLegend	103047	Rat IgG2b
Rat anti-mouse CD206	PE-Dazzle594	C068C2	BioLegend	141732	Rat IgG2a
Rat anti-mouse CD206	BV711	C068C2	BioLegend	141727	Rat IgG2a
Rat anti-mouse Ly6G	APC	1A8	BioLegend	127614	Rat IgG2a
Rat anti-mouse Ly6G	APC-Cy7	1A8	BioLegend	127624	Rat IgG2a
Rat anti-mouse CD86	APC-Fire750	GL-1	BioLegend	105045	Rat IgG2
Viability dye	eFluor506	-	Invitrogen	65-0866-14	-

Acknowledgements: We thank Mark Liebi and the animal caretakers of the ZEMB for their precious help with genotyping and mouse housing. We are grateful to Dr. Israel F. Charo (UCSF, USA) and Dr. Richard Ransohoff (Boston, USA) for providing the $CX3CR1^{GFP/+}$//$CCR2^{RFP/+}$ reporter mouse line and to Dr. Elisabetta Dejana (Milan, Italy) for providing the JAM-$A^{-/-}$ mouse line. We thank the reviewers for their excellent and productive feed-back.
Open access funding provided by Universitat Bern.

Conflict of interest: The authors declare no competing interests.

Author contributions: KB and JM performed and analysed experiments, made the figures and wrote the first draft of the manuscript; ST, CB, DI performed and analysed experiments; GE, RL, GL supervised and helped with experiments and contributed to conceptualization. UD managed the mouse breedings and genotyping. BE conceptualized and supervised the study, wrote the final version of the manuscript and obtained funding.

Funding information: Swiss National Science Foundation, Grants Numbers: 31003A_118390 and 31003A_133092; National Multiple Sclerosis Society (USA); Swiss Multiple Sclerosis Society and the Marie Sklodowska-Curie Training Network ENTRAIN as part of the Horizon 2020 Framework Program of the European Union, Grant Number: H2020-ITN-2018-813294_ENTRAIN

Ethics statement: Animal procedures were performed in accordance with the Swiss legislation on the protection of animals and were approved by the veterinary office of the Kanton Bern (permit No. BE 76/07, BE 79/10, BE 138/20).

Data availability statement: The data that support the findings of this study are available from the corresponding author upon reasonable request.

Peer review: The peer review history for this article is available at https://publons.com/publon/10.1002/eji.202350761

References

1 **Liebner, S., Dijkhuizen, R. M., Reiss, Y., Plate, K. H., Agalliu, D. and Constantin, G.**, Functional morphology of the blood–brain barrier in health and disease. *Acta. Neuropathol.* 2018. **135**: 311–336.

2 **Engelhardt, B., Vajkoczy, P. and Weller, R. O.**, The movers and shapers in immune privilege of the CNS. *Nat. Immunol.* 2017. **18**: 123–131.

3 **Hannocks, M. J., Zhang, X., Gerwien, H., Chashchina, A., Burmeister, M., Korpos, E., Song, J. et al.**, The gelatinases, MMP-2 and MMP-9, as fine tuners of neuroinflammatory processes. *Matrix Biol.* 2019. **75–76**: 102–113.

4 **Owens, T., Bechmann, I. and Engelhardt, B.**, Perivascular spaces and the two steps to neuroinflammation. *J. Neuropathol. Exp. Neurol.* 2008. **67**: 1113–1121.

5 **Marchetti, L. and Engelhardt, B.**, Immune cell trafficking across the blood-brain barrier in the absence and presence of neuroinflammation. *Vasc. Biol.* 2020. **2**: H1–18.

6 **Castro Dias, M., Odriozola Quesada, A., Soldati, S., Bo, F., Gruber, I., Hildbrand, T., Sönmez, D. et al.**, Brain endothelial tricellular junctions as novel sites for T cell diapedesis across the blood-brain barrier. *J. Cell Sci.* 2021. **134**: jcs253880.

7 **Lutz, S. E., Smith, J. R., Kim, D. H., Olson, C. V. L., Ellefsen, K., Bates, J. M., Gandhi, S. P. et al.**, Caveolin1 is required for Th1 cell infiltration, but not tight junction remodeling, at the blood-brain barrier in autoimmune neuroinflammation. *Cell Rep.* 2017. **21**: 2104–2117.

8 **Abadier, M., Haghayegh Jahromi, N., Cardoso Alves, L., Boscacci, R., Vestweber, D., Barnum, S., Deutsch, U. et al.**, Cell surface levels of endothelial ICAM-1 influence the transcellular or paracellular T-cell diapedesis across the blood-brain barrier. *Eur. J. Immunol.* 2015. **45**: 1043–1058.

9 **Marchetti, L., Francisco, D., Soldati, S., Haghayegh Jahromi N., Barcos, S., Gruber, I., Pareja, J. R. et al.**, ACKR1 favors transcellular over paracellular T-cell diapedesis across the blood-brain barrier in neuroinflammation in vitro. *Eur. J. Immunol.* 2022. **52**: 161–177.

10 **Dias, M. C., Mapunda, J. A., Vladymyrov, M. and Engelhardt, B.**, Structure and junctional complexes of endothelial, epithelial and glial brain barriers. *Int. J. Mol. Sci.* 2019. **20**: 5372.

11 **Tietz, S. and Engelhardt, B.**, Brain barriers: crosstalk between complex tight junctions and adherens junctions. *J. Cell Biol.* 2015. **209**: 493–506.

12 **Nitta, T., Hata, M., Gotoh, S., Seo, Y., Sasaki, H., Hashimoto, N., Furuse, M. et al.**, Size-selective loosening of the blood-brain barrier in claudin-5-deficient mice. *J. Cell Biol.* 2003. **161**: 653–660.

13 **Saitou, M., Furuse, M., Sasaki, H., Schulzke, J. D., Fromm, M., Takano, H., Noda, T. et al.**, Complex phenotype of mice lacking occludin, a component of tight junction strands. *Mol. Biol. Cell* 2000. **11**: 4131–4142.

14 **Ebnet, K., Suzuki, A., Horikoshi, Y., Hirose, T., Meyer Zu Brickwedde, M. K., Ohno, S. and Vestweber, D.**, The cell polarity protein ASIP/PAR-3 directly associates with junctional adhesion molecule (JAM). *EMBO J.* 2001. **20**: 3738–3748.

15 **Ebnet, K., Aurrand-Lions, M., Kuhn, A., Kiefer, F., Butz, S., Zander, K., Brickwedde, M.-K. M. Z. et al.**, The junctional adhesion molecule (JAM) family members JAM-2 and JAM-3 associate with the cell polarity protein PAR-3: a possible role for JAMs in endothelial cell polarity. *J. Cell Sci.* 2003. **116**: 3879–3891.

16 **Williams, L. A., Martin-Padura, I., Dejana, E., Hogg, N. and Simmons, D. L.**, Identification and characterisation of human junctional adhesion molecule (JAM). *Mol. Immunol.* 1999. **36**: 1175–1188.

17 **Martìn-Padura, I., Lostaglio, S., Schneemann, M., Williams, L., Romano, M., Fruscella, P., Panzeri, C. et al.**, Junctional adhesion molecule, a novel member of the immunoglobulin superfamily that distributes at intercellular junctions and modulates monocyte transmigration. *J. Cell Biol.* 1998. **142**: 117–127.

18 **Steinbacher, T., Kummer, D. and Ebnet, K.**, Junctional adhesion molecule-a: functional diversity through molecular promiscuity. *Cell Mol. Life Sci.* 2018. **75**: 1393–1409.

19 **Liu, Y., Nusrat, A., Schnell, F. J., Reaves, T. A., Walsh, S., Pochet, M. and Parkos, C. A.**, Human junction adhesion molecule regulates tight junction resealing in epithelia. *J. Cell Sci.* 2000. **113**: 2363–2374.

20 **Mandell, K. J., Holley, G. P., Parkos, C. A. and Edelhauser, H. F.**, Antibody blockade of junctional adhesion molecule-A in rabbit corneal endothelial tight junctions produces corneal swelling. *IOVS* 2006. **47**: 2408–2416.

21 **Ebnet, K.**, Organization of multiprotein complexes at cell-cell junctions. *Histochem. Cell Biol.* 2008. **130**: 1–20.

22 **Cera, M. R., Del Prete, A., Vecchi, A., Corada, M., Martin-Padura, I., Motoike, T., Tonetti, P. et al.**, Increased DC trafficking to lymph nodes and contact hypersensitivity in junctional adhesion molecule-A–deficient mice. *J. Clin. Invest.* 2004. **114**: 729–738.

23 **Klingensmith, N. J., Fay, K. T., Swift, D. A., Bazzano, J. M. R., Lyons, J. D., Chen, C. W. and Meng, M.**, Junctional adhesion molecule-A deletion increases phagocytosis and improves survival in a murine model of sepsis. *JCI. Insight*. 2022. **7**: e156255.

24 **Weber, C., Fraemohs, L. and Dejana, E.**, The role of junctional adhesion molecules in vascular inflammation. *Nat. Rev. Immunol.* 2007. **7**: 467–477.

25 **Bazzoni, G.**, Pathobiology of junctional adhesion molecules. *Antioxid. Redox. Signal.* 2011. **15**: 1221–1234.

26 **Ebnet, K., Suzuki, A., Ohno, S. and Vestweber, D.**, Junctional adhesion molecules (JAMs): more molecules with dual functions? *J. Cell Sci.* 2004. **117**: 19–29.

27 **Ostermann, G., Weber, K. S. C., Zernecke, A., Schröder, A. and Weber, C.**, JAM-I is a ligand of the β2 integrin LFA-I involved in transendothelial migration of leukocytes. *Nat. Immunol.* 2002. **3**: 151–158.

28 **Aurrand-Lions, M., Johnson-Leger, C., Wong, C., Du Pasquier, L. and Imhof, B. A.**, Heterogeneity of endothelial junctions is reflected by differential expression and specific subcellular localization of the three JAM family members. *Blood* 2001. **98**: 3699–3707.

29 **Stamatovic, S. M., Sladojevic, N., Keep, R. F. and Andjelkovic, A. V.**, Relocalization of junctional adhesion molecule a during inflammatory stimulation of brain endothelial cells. *Mol. Cell Biol.* 2012. **32**, 3414–3427.

30 **Laukoetter, M. G., Nava, P., Lee, W. Y., Severson, E. A., Capaldo, C. T., Babbin, B. A., Williams, I. R. et al.**, JAM-A regulates permeability and inflammation in the intestine in vivo. *J. Exp. Med.* 2007. **204**: 3067–3076.

31 **Mandell, K. J., McCall, I. C. and Parkos, C. A.**, Involvement of the junctional adhesion molecule-1 (JAM1) homodimer interface in regulation of epithelial barrier function. *J. Biol. Chem.* 2004. **279**: 16254–16262.

32 **Mandell, K. J., Berglin, L., Severson, E. A., Edelhauser, H. F. and Parkos, C. A.**, Expression of JAM-A in the human corneal endothelium and retinal pigment epithelium: localization and evidence for role in barrier function. *IOVS* 2007. **48**: 3928–3936.

33 **Yeung, D., Manias, J. L., Stewart, D. J. and Nag, S.**, Decreased junctional adhesion molecule-A expression during blood-brain barrier breakdown. *Acta. Neuropathol.* 2008. **115**: 635–642.

34 **Padden, M., Leech, S., Craig, B., Kirk, J., Brankin, B. and McQuaid, S.**, Differences in expression of junctional adhesion molecule-A and β-catenin in multiple sclerosis brain tissue: increasing evidence for the role of tight junction pathology. *Acta. Neuropathol.* 2007. **113**: 177–186.

35 **Plumb, J., McQuaid, S., Mirakhur, M. and Kirk, J.**, Abnormal endothelial tight junctions in active lesions and normal-appearing white matter in multiple sclerosis. *Brain Pathol.* 2002. **12**: 154–169.

36 **Kirk, J., Plumb, J., Mirakhur, M. and McQuaid, S.**, Tight junctional abnormality in multiple sclerosis white matter affects all calibres of vessel and is associated with blood-brain barrier leakage and active demyelination. *J. Pathol.* 2003. **201**: 319–327.

37 **Wang, J. and Liu, H.**, The roles of junctional adhesion molecules (JAMs) in cell migration. *Front. Cell Dev. Biol.* 2022. **10**: 843671.

38 **Cera, M. R., Fabbri, M., Molendini, C., Corada, M., Orsenigo, F., Rehberg, M., Rehberg, M. et al.**, JAM-A promotes neutrophil chemotaxis by controlling integrin internalization and recycling. *J. Cell Sci.* 2009. **122**: 268–277.

39 **Schmitt, M. M. N., Megens, R. T. A., Zernecke, A., Bidzhekov, K., Van Den Akker, N. M., Rademakers, T., van Zandvoort, M. A. et al.**, Endothelial junctional adhesion molecule-a guides monocytes into flow-dependent predilection sites of atherosclerosis. *Circulation* 2014. **129**: 66–76.

40 **Ozaki, H., Ishii, K., Horiuchi, H., Arai, H., Kawamoto, T., Okawa, K., Iwamatsu, A. et al.**, Cutting edge: combined treatment of TNF-α and IFN-γ causes redistribution of junctional adhesion molecule in human endothelial cells. *J. Immunol.* 1999. **163**: 553–557.

41 **Martinez-Estrada, O., Manzi, L., Tonetti, P., Dejana, E. and Bazzoni, G.**, Opposite effects of tumor necrosis factor and soluble fibronectin on junctional adhesion molecule-A in endothelial cells. *Am. J. Physiol. Lung. Cell. Mol. Physiol.* 2005. **288**: L1081–L1088.

42 **Steiner, O., Coisne, C., Engelhardt, B. and Lyck, R.**, Comparison of immortalized bEnd5 and primary mouse brain microvascular endothelial cells as in vitro blood-brain barrier models for the study of T cell extravasation. *J. Cereb. Blood Flow Metab.* 2011. **31**: 315–327.

43 **Ostermann, G., Fraemohs, L., Baltus, T., Schober, A., Lietz, M., Zernecke, A., Liehn, E. A. et al.**, Involvement of JAM-A in mononuclear cell recruitment on inflamed or atherosclerotic endothelium: inhibition by soluble JAM-A. *Arterioscler. Thromb. Vasc. Biol.* 2005. **25**: 729–735.

44 **Del Maschio, A., De Luigi, A., Martin-Padura, I., Brockhaus, M., Bartfai, T., Fruscella, P., Adorini, L. et al.**, Leukocyte recruitment in the cerebrospinal fluid of mice with experimental meningitis is inhibited by an antibody to junctional adhesion molecule (JAM). *J. Exp. Med.* 1999. **190**: 1351–1356.

45 **Saederup, N., Cardona, A. E., Croft, K., Mizutani, M., Cotleur, A. C., Tsou, C. L., Ransohoff, R. M. et al.**, Selective chemokine receptor usage by

central nervous system myeloid cells in CCR2-red fluorescent protein knock-in mice. *PLoS One* 2010. **5**: e13693.

46 **Pong, W. W., Walker, J., Wylie, T., Magrini, V., Luo, J., Emnett, R. J., Choi, J. et al.**, F11R is a novel monocyte prognostic biomarker for malignant glioma. *PLoS One* 2013. **8**: e77571.

47 **Turaga, S. M., Silver, D. J., Bayik, D., Paouri, E., Peng, S., Lauko, A., Choi, J. et al.**, JAM-A functions as a female microglial tumor suppressor in glioblastoma. *Neuro. Oncol.* 2020. **22**: 1591–1601.

48 **Amatruda, M., Chapouly, C., Woo, V., Safavi, F., Zhang, J., Dai, D., Therattil, A. et al.**, Astrocytic junctional adhesion molecule-A regulates T-cell entry past the glia limitans to promote central nervous system autoimmune attack. *Brain Comm.* 2022. **4**: fcac044.

49 **Sixt, M., Engelhardt, B., Pausch, F., Hallmann, R., Wendler, O. and Sorokin, L. M.**, Endothelial cell laminin isoforms, laminins 8 and 10, play decisive roles in T cell recruitment across the blood-brain barrier in experimental autoimmune encephalomyelitis. *J. Cell Biol.* 2001. **153**: 933–945.

50 **Vorbrodt, A. W. and Dobrogowska, D. H.**, Molecular anatomy of intercellular junctions in brain endothelial and epithelial barriers: electron microscopist's view. *Brain Res. Rev.* 2003. **42**: 221–242.

51 **Leech, S., Kirk, J., Plumb, J. and McQuaid, S.**, Persistent endothelial abnormalities and blood-brain barrier leak in primary and secondary progressive multiple sclerosis. *Neuropathol. Appl. Neurobiol.* 2007. **33**: 86–98.

52 **Ogasawara, N., Kojima, T., Go, M., Fuchimoto, J., Kamekura, R., Koizumi, J. I., Ohkuni, T. et al.**, Induction of JAM-A during differentiation of human THP-1 dendritic cells. *Biochem. Biophys. Res. Commun.* 2009. **389**: 543–549.

53 **Pfeiffer, F., Kumar, V., Butz, S., Vestweber, D., Imhof, B. A., Stein, J V. and Engelhardt, B.**, Distinct molecular composition of blood and lymphatic vascular endothelial cell junctions establishes specific functional barriers within the peripheral lymph node. *Eur. J. Immunol.* 2008. **38**: 2142–2155.

54 **Coisne, C., Dehouck, L., Faveeuw, C., Delplace, Y., Miller, F., Landry, C., Morissette, C. et al.**, Mouse syngenic in vitro blood-brain barrier model: a new tool to examine inflammatory events in cerebral endothelium. *Lab. Invest.* 2005. **85**: 734–746.

55 **Kakogiannos, N., Ferrari, L., Giampietro, C., Scalise, A. A., Maderna, C., Ravà, M., Taddei, A. et al.**, JAM-A acts via C/EBP-α to promote claudin-5 expression and enhance endothelial barrier function. *Circ. Res.* 2020. **127**: 1056–1073.

56 **Thölmann, S., Seebach, J., Otani, T., Florin, L., Schnittler, H., Gerke, V., Furuse, M. et al.**, JAM-A interacts with α3β1 integrin and tetraspanins CD151 and CD9 to regulate collective cell migration of polarized epithelial cells. *Cell Mol. Life Sci.* 2022. **79**: 88.

57 **Bazzoni, G., Tonetti, P., Manzi, L., Cera, M. R., Balconi, G. and Dejana, E.**, Expression of junctional adhesion molecule-A prevents spontaneous and random motility. *J. Cell Sci.* 2005. **118**: 623–632.

58 **Manes, T. D. and Pober, J. S.**, Identification of endothelial cell junctional proteins and lymphocyte receptors involved in transendothelial migration of human effector memory CD4 + T cells. *J. Immunol.* 2011. **186**: 1763–1768.

59 **Steiner, O., Coisne, C., Cecchelli, R., Boscacci, R., Deutsch, U., Engelhardt, B., Lyck, R. et al.**, Differential roles for endothelial ICAM-1, ICAM-2, and VCAM-1 in shear-resistant T cell arrest, polarization, and directed crawling on blood–brain barrier endothelium. *J. Immunol.* 2010.**185**: 4846–4855.

60 **Cunningham, S. A., Rodriguez, J. M., Pia Arrate, M., Tran, T. M. and Brock, T. A.**, JAM2 interacts with α4β1. Facilitation by JAM3. *J. Biol. Chem.* 2002. **277**: 27589–27592.

61 **Woodfin, A., Voisin, M. B., Imhof, B. A., Dejana, E., Engelhardt, B. and Nourshargh, S.**, Endothelial cell activation leads to neutrophil transmigration as supported by the sequential roles of ICAM-2, JAM-A, and PECAM-1. *Blood* 2009. **113**: 6246–6257.

62 **Woodfin, A., Reichel, C. A., Khandoga, A., Corada, M., Voisin, M. B., Scheiermann, C., Haskard, D. O. et al.**, JAM-A mediates neutrophil transmigration in a stimulus-specific manner in vivo: evidence for sequential roles for JAM-A and PECAM-1 in neutrophil transmigration. *Blood* 2007. **110**: 1848–1856.

63 **Gu, L., Tseng, S. C. and Rollins, B. J.**, Monocyte chemoattractant protein-1. *Chemokines. Chem. Immunol. Basel. Karger.* 1999. **72**: 7–29.

64 **Corada, M., Chimenti, S., Cera, M. R., Vinci, M., Salio, M., Fiordaliso, F., De Angelis, N. et al.**, Junctional adhesion molecule-A-deficient polymorphonuclear cells show reduced diapedesis in peritonitis and heart ischemia-reperfusion injury. *Proc. Natl. Acad. Sci.* 2005. **102**: 10634–10639.

65 **Bernhagen, J., Krohn, R., Lue, H., Gregory, J. L., Zernecke, A., Koenen, R. R., Dewor, M. et al.**, MIF is a noncognate ligand of CXC chemokine receptors in inflammatory and atherogenic cell recruitment. *Nat. Med.* 2007. **13**: 587–596.

66 **Agrawal, S., Anderson, P., Durbeej, M., Van Rooijen, N., Ivars, F., Opdenakker, G., Sorokin, L. M. et al.**, Dystroglycan is selectively cleaved at the parenchymal basement membrane at sites of leukocyte extravasation in experimental autoimmune encephalomyelitis. *J. Exp. Med.* 2006. **203**: 1007–1016.

67 **Song, J., Wu, C., Korpos, E., Zhang, X., Agrawal, S. M., Wang, Y., Faber, C. et al.**, Focal MMP-2 and MMP-9 activity at the blood-brain barrier promotes chemokine-induced leukocyte migration. *Cell Rep.* 2015. **10**: 1040–1054.

68 **Tietz, S., Périnat, T., Greene, G., Enzmann, G., Deutsch, U., Adams, R., Imhof, B. et al.**, Lack of junctional adhesion molecule (JAM)-B ameliorates experimental autoimmune encephalomyelitis. *Brain Behav. Immun.* 2018. **73**: 3–20.

69 **Horng, S., Therattil, A., Moyon, S., Gordon, A., Kim, K., Argaw, A. T., Hara, Y. et al.**, Astrocytic tight junctions control inflammatory CNS lesion pathogenesis. *J. Clin. Invest.* 2017. **127**: 3136–3151.

70 **Hasel, P., Cooper, M., Marchildon, A., Rufen-Blanchette, U., Kim, R., Ma, T., Kang, U. J. et al.** *Defining the molecular identity and morphology of glia limitans superficialis astrocytes in mouse and human*. Biorxiv. 2023.

71 **Wlodarczyk, A., Benmamar-Badel, A., Cédile, O., Jensen, K. N., Kramer, I., Elsborg, N. B. and Owens, T.**, CSF1R stimulation promotes increased neuroprotection by CD11c+ microglia in EAE. *Front. Cell Neurosci.* 2019. **12**: 1–10.

72 **Wlodarczyk, A., Løbner, M., Cédile, O. and Owens, T.**, Comparison of microglia and infiltrating CD11c+ cells as antigen presenting cells for T cell proliferation and cytokine response. *J. Neuroinflammation* 2014. **11**: 1–9.

73 **Arnett, H. A., Wang, Y., Matsushima, G. K., Suzuki, K. and Ting, J. P. Y.**, Functional genomic analysis of remyelination reveals importance of inflammation in oligodendrocyte regeneration. *J. Neurosci.* 2003. **23**: 9824–9832.

74 **Bö, L., Mörk, S., Kong, P. A., Nyland, H., Pardo, C. A. and Trapp, B. D.**, Detection of MHC class II-antigens on macrophages and microglia, but not on astrocytes and endothelia in active multiple sclerosis lesions. *J. Neuroimmunol.* 1994. **51**: 135–146.

75 **Kunis, G., Baruch, K., Rosenzweig, N., Kertser, A., Miller, O., Berkutzki, T. and Schwartz, M.**, IFN-γ-dependent activation of the brain's choroid plexus for CNS immune surveillance and repair. *Brain* 2013. **136**: 3427–3440.

76 **Shechter, R., Miller, O., Yovel, G., Rosenzweig, N., London, A., Ruckh, J., Kim, K.-W. et al.**, recruitment of beneficial M2 macrophages to injured spinal cord is orchestrated by remote brain choroid plexus. *Immunity* 2013. **38**: 555–569.

77 **Ivan, D., Walthert, S. and Locatelli, G.**, *Monocyte recruitment to the inflamed central nervous system: migration pathways and distinct functional polarization*. bioRxiv. 2020.

78 **Reboldi, A., Coisne, C., Baumjohann, D., Benvenuto, F., Bottinelli, D., Lira, S., Uccelli, A. et al.**, C-C chemokine receptor 6-regulated entry of TH-17 cells into the CNS through the choroid plexus is required for the initiation of EAE. *Nat. Immunol.* 2009. **10**: 514–523.

79 **Steffen, B. J., Breier, G., Butcher, E. C., Schulz, M. and Engelhardtt, B.**, lCAM-1, VCAM-1, and MAdCAM-1 are expressed on choroid plexus epithelium but not endothelium and mediate binding of lymphocytes in vitro. *Am. J. Pathol.* 1996. **148**: 1819–1838.

80 **Lazarevic, I., Soldati, S., Mapunda, J. A., Rudolph, H., Rosito, M., de Oliveira, A. C., Enzmann, G. et al.**, The choroid plexus acts as an immune cell reservoir and brain entry site in experimental autoimmune encephalomyelitis. *Fluids Barriers. CNS* 2023. **20**: 39.

81 **Murakami, M., Francavilla, C., Torselli, I., Corada, M., Maddaluno, L., Sica, A., Iliev, I. D. et al.**, Inactivation of junctional adhesion molecule-A enhances antitumoral immune response by promoting dendritic cell and T lymphocyte infiltration. *Cancer Res.* 2010. **70**: 1759–1765.

82 **Tietz, S. M., Zwahlen, M., Haghayegh Jahromi, N., Baden, P., Lazarevic, I., Enzmann, G. and Engelhardt, B.**, Refined clinical scoring in comparative EAE studies does not enhance the chance to observe statistically significant differences. *Eur. J. Immunol.* 2016. **46**: 2481–2483.

83 **Lyck, R., Ruderisch, N., Moll, A. G., Steiner, O., Cohen, C. D., Engelhardt, B., Makrides, V. et al.**, Culture-induced changes in blood-brain barrier transcriptome: implications for amino-acid transporters in vivo. *J. Cereb. Blood Flow. Metab.* 2009. **29**: 1491–1502.

84 **Engelhardt, B., Laschinger, M., Schulz, M., Samulowitz, U., Vestweber, D. and Hoch, G.**, The development of experimental autoimmune encephalomyelitis in the mouse requires α4-integrin but Not α4 β7-integrin. *J. Clin. Invest.* 1998. **102**: 2096–2105.

85 **Coisne, C., Lyck, R. and Engelhardt, B.**, Live cell imaging techniques to study T cell trafficking across the blood-brain barrier in vitro and in vivo. *Fluids Barriers CNS* 2013. **10**: 7.

86 **Wimmer, I., Tietz, S., Nishihara, H., Deutsch, U., Sallusto, F., Gosselet, F., Lyck, R. et al.**, PECAM-1 stabilizes blood-brain barrier integrity and favors paracellular T-cell diapedesis across the blood-brain barrier during neuroinflammation. *Front. Immunol.* 2019. **10**: 711.

87 **Röhnelt, R. K., Hoch, G., Reiß, Y. and Engelhardt, B.**, Immunosurveillance modelled in vitro: naive and memory T cells spontaneously migrate across unstimulated microvascular endothelium. *Int. Immunol.* 1997. **9**: 435–450.

88 **Reiss, Y., Hoch, G., Deutsch, U. and Engelhardt, B.**, T cell interaction with ICAM-1-deficient endothelium in vitro: essential role for ICAM-1 and ICAM-2 in transendothelial migration of T cells. *Eur. J. Immunol.* 1998. **28**: 3086–3099.

89 **Uboldi, C., Döring, A., Alt, C., Estess, P., Siegelman, M. and Engelhardt, B.**, L-selectin-deficient SJL and C57BL/6 mice are not resistant to experimental autoimmune encephalomyelitis. *Eur. J. Immunol.* 2008. **38**: 2156–2167.

90 **Martin-Blondel, G., Pignolet, B., Tietz, S., Yshii, L., Gebauer, C., Perinat, T., Van Weddingen, L. et al.**, Migration of encephalitogenic CD8 T cells into the central nervous system is dependent on the α4β1-integrin. *Eur. J. Immunol.* 2015. **45**: 3302–3312.

91 **Cecchelli, R., Aday, S., Sevin, E., Almeida, C., Culot, M., Dehouck, L., Engelhardt, B. et al.**, A stable and reproducible human blood-brain barrier model derived from hematopoietic stem cells. *PLoS One* 2014. **9**: e99733.

92 **Castro Dias, M., Coisne, C., Lazarevic, I., Baden, P., Hata, M., Iwamoto, N., Francisco, D. M. F. et al.**, Claudin-3-deficient C57BL/6J mice display intact brain barriers. *Sci. Rep.* 2019. **9**: 203.

93 **Lazarevic, I. and Engelhardt, B.**, Modeling immune functions of the mouse blood-cerebrospinal fluid barrier in vitro: primary rather than immortalized mouse choroid plexus epithelial cells are suited to study immune cell migration across this brain barrier. *Fluids. Barriers CNS* 2016. **13**: 2.

94 **Hsu, M., Rayasam, A., Kijak, J. A., Choi, Y. H., Harding, J. S., Marcus, S. A., Marcus, S. A., et al.**, Neuroinflammation-induced lymphangiogenesis near the cribriform plate contributes to drainage of CNS-derived antigens and immune cells. *Nat. Commun.* 2019. **10**: 229.

95 **Deutsch, U., Schlaeger, T. M., Dehouck, B., Döring, A., Tauber, S., Risau, W. and Engelhardt, B.**, Inducible endothelial cell-specific gene expression in transgenic mouse embryos and adult mice. *Exp. Cell Res.* 2008. **314**: 1202–1216.

96 **Lord, S. J., Velle, K. B., Dyche Mullins, R. and Fritz-Laylin, L. K.**, Superplots: communicating reproducibility and variability in cell biology. *J. Cell Biol.* 2020. **219**: e202001064.

97 **Martìn-Padura, I., Lostaglio, S., Schneemann, M., Williams, L., Romano, M., Fruscella, P. et al.**, Junctional adhesion molecule, a novel member of the immunoglobulin superfamily that distributes at intercellular junctions and modulates monocyte transmigration. *J. Cell Biol.* 1998. **142**: 117–127.

98 **Aurrand-Lions, M., Duncan, L., Ballestrem, C. and Imhof, B. A.**, JAM-2, a novel immunoglobulin superfamily molecule, expressed by endothelial and lymphatic cells. *J. Biol Chem.* 2001. **276**: 2733–2741.

99 **Lamagna, C., Hodivala-Dilke, K. M., Imhof, B. A. and Aurrand-Lions, M.**, Antibody against junctional adhesion molecule-c inhibits angiogenesis and tumor growth. *Cancer Res.* 2005. **65**: 5703–5710.

100 **Hahne, M., Lenter, M., Jäger, U., Isenmann, S., Vestweber, D.**, VCAM-1 is not involved in LPAM-1 (alpha 4 beta p/alpha 4 beta 7) mediated binding of lymphoma cells to high endothelial venules of mucosa-associated lymph nodes. *Eur. J. Cell Biol.* 1993. **61**: 290–298.

101 **Wimmer, I., Tietz, S., Nishihara, H., Deutsch, U., Sallusto, F., Gosselet, F. et al.**, PECAM-1 stabilizes blood-brain barrier integrity and favors paracellular T-cell diapedesis across the blood-brain barrier during neuroinflammation. *Front. Immunol.* 2019. **10**: 711.

Abbreviations: **aEAE**: active experimental autoimmune encephalomyelitis · **BBB**: blood-brain barrier · **BMDM**: bone marrow-derived macrophages · **ChP**: choroid plexus · **CNS**: central nervous system · **JAM**: junctional adhesion molecule · **MOG**: myelin oligodendrocyte glycoprotein · **MS**: multiple sclerosis · **PECAM-1**: platelete-endothelial cell adhesion molecule 1 · **pMBMEC**: primary mouse brain microvascular endothelial cells · **WT**: wildtype

Full correspondence: Prof. Dr. Britta Engelhardt, Theodor Kocher Institute, University of Bern, Freiestrasse 1, CH-3012 Bern, Switzerland
e-mail: britta.engelhardt@unibe.ch

Current address: Julia Michel, CSL Behring, Bern, Switzerland.
Silvia Tietz, GenXBioscience, Bern, Switzerland.
Daniela Ivan and Giuseppe Locatelli, Novartis, Basel, Switzerland.

Received: 7/9/2023
Revised: 11/3/2024
Accepted: 12/3/2024
Accepted article online: 18/3/2024